Exploring the aging effect of the anticancer drugs doxorubicin and mitoxantrone on cardiac mitochondrial proteome using a murine model

Sofia Reis Brandão, Ana Reis-Mendes, Pedro Domingues, José Alberto Duarte, Maria Lourdes Bastos, Félix Carvalho, Rita Ferreira, Vera Marisa Costa

PII: S0300-483X(21)00175-X

DOI: https://doi.org/10.1016/j.tox.2021.152852

Reference: TOX 152852

To appear in: *Toxicology*

Received Date: 10 April 2021

Revised Date: 2 July 2021

Accepted Date: 6 July 2021

Please cite this article as: Brandão SR, Reis-Mendes A, Domingues P, Duarte JA, Bastos ML, Carvalho F, Ferreira R, Costa VM, Exploring the aging effect of the anticancer drugs doxorubicin and mitoxantrone on cardiac mitochondrial proteome using a murine model, *Toxicology* (2021), doi: https://doi.org/10.1016/j.tox.2021.152852

Exploring the aging effect of the anticancer drugs doxorubicin and mitoxantrone on cardiac mitochondrial proteome using a murine model

Sofia Reis Brandão[1, 2], Ana Reis-Mendes[1], Pedro Domingues[2], José Alberto Duarte[3, 4], Maria Lourdes Bastos[1], Félix Carvalho[1], Rita Ferreira[2], Vera Marisa Costa[1*]

[1]UCIBIO, REQUIMTE, Laboratory of Toxicology, Department of Biological Sciences, Faculty of Pharmacy, University of Porto;
[2]LAQV-REQUIMTE, Department of Chemistry, University of Aveiro;
[3]CIAFEL, Faculty of Sports, University of Porto;
[4]IINFACTS - Institute of Research and Advanced Training in Health Sciences and Technologies, Department of Sciences, University Institute of Health Sciences (IUCS), CESPU.

*** Corresponding Author e-mail**
Vera Marisa Costa – veramcosta@ff.up.pt

UCIBIO/REQUIMTE, Laboratório de Toxicologia,
Faculdade de Farmácia, Universidade do Porto
Rua de Jorge Viterbo Ferreira, 228,
4050-313 Porto, Portugal

Highlights:

- MTX and DOX in clinically relevant doses cause heart mitochondrial injury
- MTX causes more pronounced mitochondrial cardiac proteomic changes than DOX
- Neither MTX- nor DOX-induced proteomic changes resemble cardiac ageing

Abstract

Current cancer therapies are successfully increasing the lifespan of cancer patients. Nevertheless, cardiotoxicity is a serious chemotherapy-induced adverse side effect. Doxorubicin (DOX) and mitoxantrone (MTX) are cardiotoxic anticancer agents, whose toxicological mechanisms are still to be identified. This study focused on DOX and MTX's cardiac mitochondrial damage and their molecular mechanisms. As a hypothesis, we also sought to compare the cardiac modulation caused by 9 mg/kg of DOX or 6 mg/kg of MTX in young adult mice (3 months old) with old control mice (aged control, 18-20 months old) to determine if DOX- and MTX-induced damage had common links with the aging process.

Cardiac homogenates and enriched mitochondrial fractions were prepared from treated and control animals and analyzed by immunoblotting and enzymatic assays. Enriched mitochondrial fractions were also characterized by mass spectrometry-based proteomics (GeLC-MS/MS). Data obtained showed a decrease in mitochondrial density in young adults treated with DOX or MTX and aged control, as assessed by citrate synthase (CS) activity. Furthermore, aged control had increased expression of the peroxisome proliferator-activated receptor γ coactivator 1 α (PGC1α) and manganese superoxide dismutase (MnSOD). Regarding the enriched mitochondrial fractions, DOX and MTX led to downregulation of proteins related to oxidative phosphorylation, fatty acid oxidation, amino acid metabolic process, and tricarboxylic acid cycle. MTX had a greater impact on malate dehydrogenase (MDH2) and pyruvate dehydrogenase E1 component subunit α (PDHA1). No significant proteomic changes were observed in the enriched mitochondrial fractions of aged control when compared to young control. To conclude, DOX and MTX promoted changes in several mitochondrial-related proteins in young adult mice, but none resembling the aged phenotype.

Keywords: cardiotoxicity, mitochondria dynamics, doxorubicin, mitoxantrone, ageing.

Abbreviations

ATPB: ATP synthase subunit β

ATG5: autophagy protein 5

CS: citrate synthase

Cyt c: cytochrome c

DOX: doxorubicin

ETFDH: electron transfer flavoprotein-ubiquinone oxidoreductase

GAPDH: glyceraldehyde-3-phosphate dehydrogenase

GeLC-MS/MS: mass spectrometry-based proteomics

HADHB: trifunctional enzyme subunit beta

HSPD1: 60 kDa heat shock protein

IDH3A: isocitrate dehydrogenase [NAD] subunit α

MDH2: malate dehydrogenase

MIC60: MICOS complex subunit Mic60

MnSOD: manganese superoxide dismutase

MS: mass spectrometry

mtDNA: mitochondrial DNA

MTX: mitoxantrone

OGCP: 2-oxoglutarate/malate carrier protein

OXPHOS: oxidative phosphorylation

PGC1α: peroxisome proliferator-activated receptor γ coactivator 1 α

ROS: reactive oxygen species

SERCA2: sarcoplasmic/endoplasmic reticulum calcium ATPase 2

SUCLA2: succinate--CoA ligase [ADP-forming] subunit beta

tDNA: total DNA

TEM: transmission electronic microscopy

Top2: topoisomerase II

VDAC1: voltage-dependent anion-selective channel protein 1

VLCAD: very long-chain specific acyl-CoA dehydrogenase

1. Introduction

In recent years, the life span of cancer patients has increased considerably, thanks to better cancer therapies and earlier diagnosis (Siegel et al., 2019). Among the multiple anticancer drugs available, doxorubicin (DOX) and mitoxantrone (MTX), two topoisomerase II (Top2) inhibitors, are commonly used to treat solid cancers, leukemia and lymphomas (Citron et al., 2003; Jain and Aronow, 2019; Löwenberg et al., 1998). Unfortunately, these agents are not selective and they also affect non-cancerous cells, leading to adverse side effects, such as fatigue, alopecia, myelosuppression, mucositis, and cardiotoxicity (Jain and Aronow, 2019).

Cardiotoxicity is an important and clinically limiting side effect of chemotherapy with DOX and MTX, which can manifest as arrhythmias, electrocardiographic changes and heart failure, thus compromising the patient's life (Jain and Aronow, 2019). Cardiac homeostasis largely depends on mitochondria. For several decades, it has been known that DOX can accumulate in cardiac mitochondria, forming complexes with cardiolipin (Pereira et al., 2016). Moreover, interaction with this organelle also leads to redox cycling with the formation of reactive oxygen species (ROS) (Davies and Doroshow, 1986; Doroshow and Davies, 1986). Although MTX also causes similar clinical cardiotoxic effects, the underlying mechanisms seem to be distinct. MTX is less prone to enter redox cycling and form ROS. Nevertheless, it has also been shown to be an important mitochondrial metabolic toxicant (Rossato et al., 2014, 2013).

Furthermore, DOX and MTX are non-selective inhibitors of Top2, and in cardiomyocytes they interact with topoisomerase IIβ (Top2β), which is present in both the nucleus and mitochondria (Low et al., 2003; Vejpongsa and Yeh, 2013). Additionally, these drugs form adducts with DNA, resulting in Top2–drug–DNA cleavage complexes that eventually induce changes in the transcriptome (Lyu et al., 2007). In accordance, mice treated with DOX show a decrease in the transcript levels of genes involved in mitochondrial biogenesis and oxidative phosphorylation (OXPHOS) and an increase in apoptosis markers, as well as an increase in the production of ROS and ultrastructural changes in mitochondria (Khiati et al., 2014; Xi et al., 2011; Zhang et al., 2012; Zhao et al., 2014). It has also been suggested that DOX and MTX interact with mitochondrial DNA (mtDNA), either directly by intercalating with it, or via mitochondrial topoisomerase 1 (Top1mt) (Ashley and Poulton, 2009; Khiati et al., 2014). DOX treatment decreased mtDNA copy number and upregulated the mitochondrial fusion dynamin-like 120 kDa protein (OPA1), while increasing mtDNA damage (Khiati et al., 2014; Yoon et al., 2018). In addition, DOX-induced cardiotoxicity has also been associated with an accumulation of iron or toxic metabolites, such as aglycones, in mitochondria, regardless of the involvement of topoisomerases (Filipa Reis-Mendes et al., 2015; Ichikawa et al., 2014).

Despite the available research data, particularly with DOX, the most relevant cardiotoxicity mechanisms of these drugs are still unclear, and integrative analysis of mitochondria can elucidate the molecular and functional changes observed in humans. There are several approaches to study mitochondrial plasticity. Mitochondrial proteomics based on mass spectrometry (MS) is a very comprehensive technique that allows the characterization of molecular processes modulated by several pathophysiological conditions (Ferreira et al., 2018, 2014; Stauch et al., 2015). Indeed, some studies have applied MS-based proteomics to explore the cardiotoxicity induced by doxorubicin using *in vivo* models (Chen et al., 2006; Cui et al., 2010; Kumar, 2011; Merten et al., 2005; Vedam et al., 2010; Xi et al., 2011; Zhao et al., 2014), but only one explored the cardiac mitochondria (Zhao et al., 2014). Moreover, proteomics after mitoxantrone has only been tested in HL-1 cells (Costa et al., 2020).

The link between mitochondria and ageing dates back more than half a century. Indeed, cardiac ROS are mediators in age-dependent cell damage, being associated with changes in lipids and proteins (proteotoxic stress), and with a high rate of mtDNA mutations. These alterations decrease mitochondrial content and disturb the mitochondrial structure, leading to an accumulation of misfolded mitochondrial proteins associated with ageing (Boengler et al., 2017; Sun et al., 2016). Other processes, such as cell senescence, inflammation, and autophagy have also been associated with loss of mitochondrial function on cardiac ageing (Ketul R et al., 2011; Sun et al., 2016). Anthracycline treatment was reported to contribute to the aging heart, including mitochondrial impairment and accumulation of damaged proteins and organelles (Ayyadevara et al., 2016; Costa et al., 2020; Dores-Sousa et al., 2015; Rossato et al., 2014; Varga et al., 2015). Furthermore, anthracycline impairs progenitor cell function and causes higher telomere shortening in the young heart (Armstrong and Ross, 2014; Chung et al., 2020; Huang et al., 2010).

Therefore, this study aimed to assess the effects of DOX and MTX, on the cardiac mitochondrial proteome, using clinically relevant cumulative doses, and a MS-based proteomic approach taken on isolated mitochondria. To this end, we used young adult male CD-1 mice given multiple administrations of DOX and MTX to assess the underlying molecular mechanisms of cardiac mitochondrial changes. In parallel, a group of elderly mice was taken to compare the studied markers with the changes induced by DOX and MTX in young adult mice, as to analyze the hypothesis that these therapies could lead to cardiac ageing.

2. Materials and Methods

2.1 Chemicals

All chemicals and reagents were of analytical grade or of the highest grade available. Acetyl coenzyme A (acetyl-CoA) sodium salt, adenosine 5′-triphosphate (ATP) disodium salt hydrate, bovine serum albumin (BSA), 5,5′-dithiobis-(2-nitrobenzoic acid) (DTNB), DL-dithiothreitol (DTT), DOX hydrochloride, ethylene glycol-bis(2-aminoethylether)-N,N,N′,N′-tetraacetic acid (EGTA), HEPES hemisodium salt, iodoacetamide, MTX dihydrochloride, phenylmethanesulfonyl fluoride (PMSF), phosphate buffered saline (PBS), Ponceau S, protease inhibitors cocktail, subtilopeptidase A type VIII, sodium chloride (NaCl), sucrose, and Tween20 were obtained from Sigma-Aldrich (St. Louis, MO, USA).

Mouse monoclonal anti-ATP synthase subunit β (ATPB, ab14730), mouse monoclonal anti-sarcoplasmic/endoplasmic reticulum calcium ATPase 2 (SERCA2, ab2861), rabbit monoclonal anti-autophagy protein 5 (ATG5, ab108327), rabbit polyclonal anti-electron transfer flavoprotein-ubiquinone oxidoreductase (ETFDH, ab91508), rabbit polyclonal anti-glyceraldehyde-3-phosphate dehydrogenase (GAPDH, ab9485), rabbit polyclonal anti-manganese superoxide dismutase (MnSOD, ab13533), rabbit polyclonal anti-MICOS complex subunit Mic60 (MIC60, ab48139), rabbit polyclonal anti-peroxisome proliferator-activated receptor γ coactivator 1 α (PGC1α, ab191838) and MitoProfile Total OXPHOS Rodent (ab110413) antibodies were obtained from Abcam (Cambridge, UK). Mouse monoclonal anti-cytochrome c (Cyt c, 556433) was obtained from BD Biosciences Pharmingen (San Jose, CA, USA). Horseradish peroxidase-conjugated anti-mouse (NA931) or anti-rabbit (NA934) antibodies were obtained from GE Healthcare (Buckinghamshire, UK). Enhanced chemiluminescence (ECL) reagent was purchased from Advansta (CA, USA) and trypsin (1862748) was obtained from Pierce, Life Technologies (Rockford, IL, USA).

2.2. Animals and experimental design

Male CD-1 mice (*Mus musculus*) were created and kept at the vivarium of Abel Salazar Institute of Biomedical Sciences of University of Porto (ICBAS-UP), under the supervision of experienced veterinarians. Mice were housed in Green Line individually ventilated cages (IVC) Sealsafe plus Mouse (GM500, Tecniplast, UK), in a maximum of three animals *per* cage, in a temperature (22 ± 2°C) and humidity-controlled environment and a 12 h light-dark cycle. Standard rodent 4RF21 certificate diet (Mucedola, Settimo Milanese, Italy) and water were provided *ad libitum*. During the entire experimental period, food and water intake, body weight and animal welfare were assessed daily.

Three months old mice (young adult, 30 animals) were used to assess DOX- and MTX-effects on cardiac mitochondria, while 18-20 months old mice were used as an elderly comparison group (aged control, 6 animals) (Dutta and Sengupta, 2016). Young adult male mice were divided into three groups: control (young control, 10 animals), young DOX (10 animals) and young MTX (10 animals) groups. Both DOX and MTX solutions were prepared in saline solution (0.9% NaCl) and in sterile conditions. Animals were administrated intraperitoneally (i.p.) twice a week for three weeks to attain a 9 mg/kg or 6 mg/kg cumulative dose for DOX or MTX, respectively. Mice in the young control group received six i.p. administrations of 0.9% NaCl in the same volume and conditions as the drug-exposed groups. The administration schedule was selected to mimic human anticancer therapy that consists of multiple administrations at separated time-points (Dores-Sousa et al., 2015). The dosages were calculated based on allometric scaling and considering the conversion factor 37 for body area surface between mice and humans, as recommended by the US Food and Drug Administration (Reagan- Shaw et al., 2008). The DOX cumulative dose of 9 mg/kg in adult mice corresponded roughly to ~50 mg/m^2, while MTX 6 mg/kg in mice corresponded to ~30 mg/m^2 in humans. Both cumulative doses set in this experiment were much lower than the maximum lifelong doses recommended for humans (DOX maximum cumulative recommended dose is 400-550 mg/m^2, while MTX maximum cumulative recommended dose is 140 mg/m^2) (Filipa Reis-Mendes et al., 2015).

One week after the last administration, mice were anesthetized with isoflurane and then sacrificed by exsanguination, as ethically determined by the guidelines. Immediately after sacrifice, the hearts were excised, weighed, and then prepared for biochemical analysis and transmission electronic microscopy (TEM).

The animal protocol was approved by the local Committee Responsible for Animal Welfare (ORBEA) of ICBAS-UP (project number 140/2015), the Portuguese Ethics Committee for Animal Experimentation (General Directorate of Food and Veterinary, reference number 0421/000/000/2016) and it was performed in accordance to European Council Directive (2010/63/EU).

2.3. Cardiac homogenates and mitochondrial enriched fractions preparation

All procedures were performed in ice. After excision, hearts were kept in PBS and then washed with isolation medium (250 mM sucrose, 0.5 mM EGTA, 10 mM HEPES-KOH, pH 7.4 and 0.1% BSA fat-free). The blood-free tissue was resuspended in isolation medium containing protease subtilopeptidase A type VIII (1 mg/g tissue) and homogenized with a tightly fitted Potter-Elvehjen homogenizer and Teflon pestle. After a 1-min incubation at 4°C, the suspension was centrifuged (14,500 *g*, 10 min, 4°C). The

supernatant was then discarded, and the pellet (essentially devoid of protease) was gently resuspended in isolation medium and homogenized, thus resulting in the cardiac homogenate. An aliquot of the cardiac homogenates was reserved for biochemical analyzes and the remaining homogenate was centrifuged (750 *g*, 10 min, 4°C). The obtained supernatant was further centrifuged (12,500 *g*, 10 min, 4°C) and the resulting pellet was resuspended in washing medium (250 mM sucrose, 10 mM HEPES-KOH, pH 7.4) and re-pelleted through centrifugation (12,500 *g*, 10 min, 4°C). The pellet containing the mitochondrial enriched fraction was gently resuspended in a washing medium containing a cocktail of protease inhibitors and PMSF. Whole cardiac homogenates and mitochondrial enriched fractions were stored at -80°C for biochemical analysis. These procedures were done as previously described (Ascensão et al., 2006).

The protein concentration of cardiac homogenates and mitochondrial enriched fractions was estimated with the commercial method RC DC Protein Assay (Bio-Rad, Hercules, CA, USA), using BSA as standard and following manufacturer's instructions.

2.4. DNA quantification

DNA quantification (n = 10 for young control, young DOX and young MTX; n = 6 for aged control) was performed using the Broad Range Assay kit compatible with Qubit fluorometer (Invitrogen, Carlsbad, CA, USA). DNA was measured separately in cardiac homogenates and mitochondrial enriched fractions. The final mtDNA-to-total DNA (tDNA) ratio was calculated considering the total volumes obtained for each biological fraction.

2.5. Evaluation of citrate synthase (CS) activity

CS activity (n = 10 for young control, young DOX and young MTX; n = 6 for aged control) was measured in both whole cardiac homogenates and mitochondrial enriched fractions according to Coore *et al*. (Coore et al., 1971). The free thiol groups of coenzyme A (CoA), which result from the reaction of acetyl-CoA with oxaloacetate, react with DTNB. The resulting 2-nitro-5-thiolbenzoate anion has a strong absorption at 412 nm (molar extinction coefficient of 13.6 $mM^{-1} \cdot cm^{-1}$). The absorbance was read at 412 nm for approximately 2 min at 30°C in a microplate reader (Multiskan GO, Thermo Fischer Scientific, Northumberland, UK). The values were normalized to total protein.

2.6. Evaluation of ATP synthase activity

ATP synthase activity (n = 10 for young control, young DOX and young MTX; n = 6 for aged control) was measured in mitochondrial enriched fractions, as previously

described (Simon et al., 2003). Phosphate produced by hydrolysis of ATP reacts with ammonium molybdate in the presence of reducing agents to form a blue color complex. The intensity of this complex is proportional to the concentration of phosphate in solution. The absorbance was read at 610 nm in a microplate reader (Multiskan GO, Thermo Fischer Scientific, Northumberland, UK). The values were normalized to total protein.

2.7. Western blotting analysis

Equal amounts of protein (20 µg; n = 6) were loaded on a 12.5% SDS-PAGE according to Laemmli (Laemmli, 1970). The resolved proteins were blotted onto a nitrocellulose membrane (Amersham Protran, GE Healthcare, Germany) for 2 h at 200 mA in transfer buffer. Protein loading was controlled by Ponceau S staining. The nonspecific binding was blocked with 5% (w/v) nonfat dry milk in Tris buffered saline with Tween20 (TBS-T). Next, the membranes were incubated with the primary antibody diluted 1:500 or 1:1000 in 5% (w/v) nonfat dry milk in TBS-T, for 2 h at room temperature or overnight at 4°C, depending on the antibody used. Anti-ATPB, Cyt c, ETFDH and SERCA2 antibodies were incubated for both whole cardiac homogenates and mitochondrial enriched fractions. ATG5, GAPDH, MnSOD and PGC1α were immunodetected only in cardiac homogenates, while MIC60 and specific subunits of OXPHOS complexes were evaluated exclusively in mitochondrial enriched fractions. For further details on the specific dilutions and samples used for each primary antibody see Supplementary Table 1. Then, membranes were washed with TBS-T and incubated with the appropriate secondary horseradish peroxidase-conjugated antibody diluted 1:1000 in 5% (w/v) nonfat dry milk in TBS-T. Membranes were exposed with ECL reagent according to the manufacturer's recommendations. The immunoreactive bands were automatically detected using the ChemiDoc Imaging System version 2.3.0.07 (Bio-Rad, Hercules, CA, USA). The images obtained were analyzed with Image Lab software version 6.0.1 (Bio-Rad, Hercules, CA, USA). The band intensity values obtained were normalized to total protein using the Ponceau S staining and expressed relative to the young control group.

2.8. Tissue preparation for transmission electron microscopy (TEM)

In young adult mice (n = 3) at the end of the experimental protocol, roughly 1 mm^3 of the ventricle was fixed in 2% glutaraldehyde (2 h, 4°C), post-fixed with 2% osmium tetroxide, dehydrated in graded ethanol and later embedded in Epon (*TAAB 812 Resin, Kit Cat. No. T024*), using routine standard procedures as already described (Rossato et al., 2014). Ultrathin (100 nm) sections obtained in an ultramicrotome (Reichert Ultracut) were mounted in copper grids (300 Mesh, from TAAB Laboratories Equipment Ltd,

England) and further contrasted with uranyl acetate and lead citrate for transmission electron microscopy analysis at an accelerating voltage of 60 kV (Jeol JEM 1400 Transmission Electron Microscope, Tokyo, Japan). Digital images were captured using a CCD digital camera Orious 1100W (Tokyo, Japan).

2.9. GeLC-MS/MS analysis of mitochondrial enriched fractions

Equal amounts of protein (30 µg; n = 4 for young control, young DOX and young MTX; n = 5 for aged control) from mitochondrial enriched fractions were separated using a 12.5% SDS-PAGE, as previously described (Laemmli, 1970). The gels were stained with Colloidal Coomassie Blue G250 and destained with 25% methanol until an optimal contrast was achieved. Then, the protein bands were cut off from the gels and *in-gel* digested with trypsin, (enzyme-to-total protein ratio of 1:20) according to Shevchenko *et al.* (Shevchenko et al., 2006). The gel pieces were reduced with 10 mM DTT and alkylated with 55 mM iodoacetamide. Next, the peptides were extracted from the gel pieces and lyophilized in a SpeedVac (SC210A; ThermoSavant Milford, MA, USA).

The tryptic peptides were resuspended in 1% formic acid (FA) and analyzed with a QExactive Orbitrap (Thermo Fisher Scientific, Bremen, Germany) through the EASY-spray nano ESI source (Thermo Fisher Scientific) that was coupled to an Ultimate 3000 (Dionex, Sunnyvale, CA) high-pressure liquid chromatography (HPLC) system. The trap column (100 µm I.D. x 2 cm packed with Acclaim PepMap RSLC C18, 5 µm 100 Å) and the EASY-spray analytical column (75 µm I.D. x 75 cm packed with Acclaim PepMap RSLC C18, 3 µm 100 Å) were from Thermo Fisher Scientific. Peptides were trapped at 30 µL/min in 96% solvent A (0.1% FA). Elution was achieved with the solvent B (0.1% FA:80% acetonitrile) at a flow rate of 300 nL/min. The 92 min gradient used was as follows: 0–3 min, 96% solvent A; 3–70 min, 4–25% solvent B; 70–90 min, 25–40% solvent B; 90–92 min, 90% solvent B; 92–100 min, 90% solvent B; 101-120 min, 96% solvent A. The mass spectrometer was operated at 1.8 kV in the data-dependent acquisition mode. A tandem MS (MS/MS) method was used with a survey scan from 400 to 1600 *m/z* (resolution 70,000; auto gain control (AGC) target 1E6). The 10 most intense peaks were subjected to higher-energy collisional dissociation to obtain MS/MS spectrum (resolution 17,500; AGC target 5E4, normalized collision energy 28%, max. injection time 100 ms and dynamic exclusion 35 s).

2.10. Protein identification and label-free quantification of GeLC-MS/MS data from mitochondrial enriched fractions

Raw spectra generated by GeLC-MS/MS were processed and analyzed using Proteome Discoverer software version 2.2 (Thermo Fisher Scientific), with the MS

Amanda (version 2.0, University of Applied Sciences Upper Austria, Research Institute of Molecular Pathology) and Sequest HT search engines. Uniprot (TrEMBL and Swiss-Prot) protein sequence database (version of October 2017) was used for all searches under *Mus musculus*. Database search parameters were as follows: carbamidomethylation of cysteine, oxidation of methionine, and the allowance for up to two missed tryptic cleavages. The peptide mass tolerance was 10 ppm and fragment ion mass tolerance was 0.02 Da. To achieve a 1% false discovery rate, the Percolator (version 2.0, Thermo Fisher Scientific) node was implemented for a decoy database search strategy and peptides were filtered for high confidence and a minimum length of 6 amino acids, and proteins were filtered for a minimum number of peptide sequences of 1. The minimal number of identified unique peptides was set to two peptides per protein. Protein grouping was attributed according to biological process using Gene Ontology database on Uniprot (http://www.uniprot.org).

2.11. Statistical analysis

The data (except for proteomics) are presented as mean ± standard deviation (SD). Statistical analysis was performed with GraphPad Prism software version 8.4.2 (GraphPad software Inc, La Jolla, CA). Experimental groups were compared using ordinary one-way ANOVA followed by Tukey's multiple comparisons test. Results were considered different when p-value<0.05 and for p-value<0.1 it was assumed that there was a tendency.

The proteomics data obtained by GeLC-MS/MS was analyzed using R version 3.5.1 in Rstudio version 1.1.4. Proteins that were identified in exclusively one sample were not considered. The missing values were replaced by 1/5 of minimum positive values of their corresponding variables. Data were normalized by EigenMS (Karpievitch et al., 2014) and subjected to pareto scaling. PCA was performed using the R libraries FactoMineR (Lê et al., 2008) and factoextra (Kassambara and Mundt, 2020). Heatmaps were created using the R package pheatmap using "Euclidean" as the clustering distance and "ward.D" as the clustering method (Kolde, 2019). All graphics and boxplots were created using the R package ggplot2 (Wickham, 2009).

3. Results

3.1. DOX and MTX modulate whole body weight and heart weight of young adult mice

Administration of MTX induced a decrease in the body weight of the treated young MTX compared with the young control group ($p<0.05$; Table 1), which was accompanied by a decrease in the heart weight ($p<0.01$). Treatment with DOX also decreased heart´s weight, compared with young control animals ($p<0.05$). Additionally, both DOX and MTX decreased the heart weight-to-brain weight ratio compared to young control animals ($p<0.001$). No significant differences in heart weight-to-whole body weight ratio were observed between the groups, despite a decreasing trend observed in young DOX compared with young control animals ($p=0.06$). On the other hand, aged control animals exhibited a significant increase in body weight ($p<0.01$) and brain weight ($p<0.001$), but not on heart weight, compared with young control mice. No significant differences were observed in the yield of isolated heart mitochondria among groups.

3.2. DOX and MTX decreased mitochondrial density on whole cardiac homogenates

To assess the impact of DOX and MTX on cardiac mitochondrial dynamics, the activity of CS, a rough indicator of mitochondrial density (Larsen et al., 2012), was measured in whole cardiac homogenates (Figure 1). Significantly lower values of CS activity were found in young DOX or young MTX compared with young control animals ($p<0.001$). The expression of PGC1α, a transcription factor involved in the regulation of mitochondrial biogenesis (Scarpulla, 2011), was also measured. No differences on the expression of PGC1α and on the PGC1α-to-CS activity ratio were observed in the hearts of the treated animals compared with the young control mice. The levels of ATG5, a protein essential in canonical and non-canonical autophagy (Ye et al., 2018), were also assessed. Additionally, and taking into account the role of the drugs in the production of ROS, the expression of the antioxidant enzyme, MnSOD, was analyzed. Administration of DOX and MTX did not caused significant differences in the levels of these proteins compared to young control mice.

Regarding the aged control mice, they exhibited a decreased activity of CS compared with the young control animals ($p<0.0001$). This decrease was apparently compensated by the increase in the content of PGC1α. Indeed, a 2-fold increase was observed in the hearts of aged control compared with young control ($p<0.01$). However, the PGC1α-to-CS activity ratio did not show significant differences between the groups. Regarding the expression of ATG5, no difference was observed in aged control compared with young control, but a tendency for higher values for aged control compared

with young DOX (p=0.06) and young MTX (p=0.07) was observed. For MnSOD, higher values were noted in aged control compared with young control (p<0.01). Moreover, aged control exhibited a significant increase in PGC1α values compared with young animals treated with DOX or MTX (p<0.01). Similarly, aged control showed increased levels of MnSOD compared to young DOX (p<0.01) and young MTX (p<0.05) mice. In addition, aged control revealed tendency to decrease the activity of CS (p=0.06) compared with young DOX mice.

3.3. DOX and MTX changed mitochondria and cardiomyocyte structure of young adult mice

At representative TEM analysis, the cardiomyocytes from young control (Figure 2A) showed a normal ultrastructure, with mitochondria of normal dimensions and shape, containing cristae with lamellar appearance, and some lipid droplets dispersed. Spread cytoplasmic deposits of glycogen were also observed. No signs of lysosomal activation or intracellular edema were detected. In the young DOX group (Figure 2B), the most notable ultrastructural changes observed were the presence of a pronounced intracellular edema, the change in the morphology of the mitochondrial cristae, with a vesicular aspect, as well as the presence of numerous primary and secondary lysosomes. In the cardiomyocytes of this group, glycogen granules were not detected, but the presence of lipid droplets was very frequent. Normal-looking cardiomyocytes were also observed nearby the affected cardiomyocytes and the greatest intensity of the ultrastructural changes occurred in the subendocardial region. In the young MTX group (Figure 2C) however, the majority of the analyzed cardiomyocytes evidenced a slight intracellular edema, suggested by the enlarged cytosolic space among organelles and myofibrils, with a great amount of primary and secondary lysosomes. A global mitochondrial swelling was also notorious. Signs of glycogen granules were not detected, which clearly contrasted with the frequent and large lipid droplets observed. Interspaced with the cardiomyocytes showing these alterations, cardiac cells with a normal ultrastructure were detected. The more pronounced ultrastructural changes after MTX were observed in cardiomyocytes located at the subendocardial region.

3.4. DOX and MTX did not induce metabolic changes on whole cardiac homogenates

The effect of DOX and MTX on the enzymes of cardiac metabolism was assessed in cardiac homogenates. The expression of ATPB, a subunit from complex V of OXPHOS, and the glycolytic enzyme GAPDH were measured. ETFDH was also evaluated as it links β-oxidation of fatty acids to OXPHOS, and the heart is highly

dependent on this metabolic pathway to obtain energy (Zhang et al., 2006). Moreover, the GAPDH-to-ATPB and ETFDH-to-ATPB ratios were determined (Figure 3).

Animals treated with DOX or MTX did not show significant differences in the content of ATPB, GAPDH and ETFDH compared with the young control mice. Similarly, these anticancer drugs did not promote significant changes in the GAPDH-to-ATPB and ETFDH-to-ATPB ratios.

On the other hand, significantly higher levels of ATPB and GAPDH ($p<0.001$) were observed in aged control compared with young control animals. In addition, aged control mice showed a tendency to increase the levels of ETFDH compared to young control ($p=0.05$). Nevertheless, no difference was seen for the GAPDH-to-ATPB and ETFDH-to-ATPB ratios in aged control. Moreover, increased levels of ATPB, GAPDH and ETFDH were found in aged control animals compared to young mice treated with DOX and MTX.

3.5. DOX and MTX contribute to proteome remodeling on cardiac mitochondrial enriched fractions

To better understand the changes observed in mitochondria after treatment with DOX or MTX, we focused our study on the proteome remodeling of this organelle. The purity of the isolated mitochondria was confirmed by Western blotting (WB) analysis of organelle-specific markers in whole cardiac homogenates and mitochondrial enriched fractions. Cyt c was increased in mitochondrial enriched fractions, whereas SERCA2, a marker of the sarcoplasmic reticulum, was almost absent, thus demonstrating the purity of these fractions (Supplementary Figure 1A).

GeLC-MS/MS analysis of the enriched mitochondrial fractions made it possible to identify 583 different proteins (Supplementary Table 2), of which 60% were assigned as mitochondrial proteins according to MitoCarta (Calvo et al., 2016). This value is consistent with previously reported data (Ferreira et al., 2018, 2014; Taylor et al., 2003), since a considerable proportion of the identified proteins are expected to have more than one subcellular location (Taylor et al., 2003).

No difference was observed among groups in the electrophoretic separation of the enriched mitochondrial fractions (Supplementary Figure 1B). Similarly, no large difference was found in the number of proteins identified among the groups (the mean number of proteins identified was respectively 324, 294, 313 and 303 for young control, aged control, young DOX and young MTX). However, PCA of proteomics data (Supplementary Table 3) demonstrated clustering among groups (Component 1: 49%, Component 2: 22.3%, Figure 4). Indeed, MTX treatment caused a more different mitochondrial protein profile from young control than DOX treatment. On the other hand,

the aged control animals induced relatively small deviations compared with young control animals.

In addition, the heatmap shows that the top 50 proteins, with the lowest *p*-values, (Figure 5) clearly classified the animals treated with DOX and MTX. Among the top 50 proteins, the major contributing biological processes were oxidative phosphorylation (10 proteins), fatty acid oxidation (9 proteins), tricarboxylic acid cycle (9 proteins) and amino acid metabolic process (4 proteins). The remaining proteins were linked to several different biological processes related to mitochondrial homeostasis.

In the boxplots of the top 16 proteins, with the lowest p-values, (Figure 6) we can see the modulation of the main processes induced by the treatment with DOX and MTX. The following proteins were found downregulated by DOX and MTX: ATPA, ATPB and ATPC which are linked to the oxidative phosphorylation process; ETFDH, very long-chain specific acyl-CoA dehydrogenase (VLCAD) and the trifunctional enzyme subunit beta (HADHB), proteins essential for the oxidation of fatty acids; succinate--CoA ligase [ADP-forming] subunit beta (SUCLA2) and isocitrate dehydrogenase [NAD] subunit α (IDH3A), which are proteins of the tricarboxylic acid cycle; and proteins from aspartate transmembrane transport (2-oxoglutarate/malate carrier protein, OGCP), ion transport (isoform PI of voltage-dependent anion-selective channel protein 1, PI.VDAC1) and mitochondrion organization (prohibitin-2, PHB2). Moreover, MTX severely downregulated malate dehydrogenase (MDH2), a protein related to the tricarboxylic acid cycle, and pyruvate dehydrogenase E1 component subunit α (PDHA1). No differences in protein levels were found for aged control compared with young control, as previously observed in the PCA and heatmap analysis.

Nevertheless, Western blot analysis of OXPHOS subunits such as succinate dehydrogenase [ubiquinone] iron-sulfur subunit (SDHB) and cytochrome c oxidase subunit 1 (COX1) which belong to the OXPHOS complex II and IV, respectively, showed no differences among the groups (Supplementary Figure 2). Additionally, no differences were found for the CS and ATP synthase activities performed on the mitochondrial enriched factions (Supplementary Figure 2).

4. Discussion

DOX and MTX are widely used as chemotherapeutic agents due to their high anticancer efficacy. However, they cause several side effects, including cardiotoxicity (Jain and Aronow, 2019). Moreover, they affect cardiac mitochondria (Filipa Reis-Mendes et al., 2015; Huang et al., 2021; Ichikawa et al., 2014; Rossato et al., 2013; Yu et al., 2020; Zhang et al., 2012), although their exact mechanisms are not yet entirely clear. Our objective was to study mitochondrial plasticity in response to these two anticancer drugs using general approaches and MS-based mitochondrial proteomics. The mechanisms underlying the cardiotoxicity of these drugs were examined in both total cardiac homogenates and mitochondrial enriched fractions. We also sought to compare the cardiac modulation caused by DOX and MTX in young adult mice (3 months) with old mice (18 - 20 months old) to reveal possible common links of DOX- and MTX-induced damage with the decreased functionality observed during the aging process.

Administration of DOX and MTX significantly decreased heart weight, as well as the ratio heart weight-to-brain weight. Changes in heart weight were previously reported in DOX treated animals (Hixon et al., 1981; Willis et al., 2019), suggesting a defective heart. Indeed, a decrease in left ventricle weight was observed in patients treated with DOX, despite no alteration found in the left ventricular ejection fraction (Jordan et al., 2019). Moreover, several studies have demonstrated cardiac perturbed function and damage after using cumulative doses ranging from 3 to 30 mg/kg for DOX and from 6 to 7.5 mg/kg for MTX (Favreau-Lessard et al., 2019; Huang et al., 2021; Reis et al., 2021; Rossato et al., 2014; Yu et al., 2020; Zhang et al., 2020). Indeed, in previous works of the group with MTX (cumulative doses of 6 and 7.5 mg/kg), areas of connective tissue and fibrosis, along with cellular infiltration, enlargement of the interstitial space and dispersed swollen cardiomyocytes with increased inter-myofibril space were observed (Reis et al., 2021; Rossato et al., 2014). Similarly, the usage of cumulative doses of 20 and 30 mg/kg of DOX led to accumulation of interstitial fibrosis, as well as numerous inflammatory cells in the heart tissue, evidencing structural cardiac changes (Huang et al., 2021; Yu et al., 2020).

Regarding whole cardiac homogenates, DOX and MTX significantly decreased mitochondrial density, given by the activity of CS, a rough indicator of mitochondrial density (Larsen et al., 2012). Several studies have reported that DOX reduced mitochondrial number and mtDNA copy number, and upregulating the mitochondrial OPA1 (Hao et al., 2015; Hixon et al., 1981; Lebrecht et al., 2003; Yoon et al., 2018). Both DOX and MTX interact with Top2β, which is essential for proper replication and transcription of tDNA and mtDNA (Low et al., 2003; Lyu et al., 2007; Vejpongsa and Yeh, 2013). However, in the present study, no difference was found for the mtDNA-to-tDNA

ratio. This ratio was calculated based on the overall contribution of DNA, without measurement of putative DNA mutations. Moreover, no differences in the expression of PGC1α, which is a key player in the regulation of mitochondrial biogenesis (Scarpulla, 2011), was observed. Thus, our experimental paradigm does not support the previously reported data on the DOX-induced reduction in mRNA and protein levels of PGC1α (Hao et al., 2015; Yang et al., 2014; Zhang et al., 2012). However, the total cumulative dose (20 mg/kg or higher) used in the previous studies was greater than our cumulative dose. Further, we explored ATG5 expression levels, as the mechanisms of autophagy and mitophagy may contribute to the decrease on mitochondrial density (Xu et al., 2018; Ye et al., 2018), and a previous report showed that DOX increased expression of autophagy markers, such as microtubule-associated light chain 3B (LC3B), sequestosome 1 (p62), and ATG5 (Xu et al., 2018). Nevertheless, no difference in ATG5 levels was found.

Both DOX- and MTX-induced changes in the cardiac mitochondrial proteome were consistent with the cardiotoxic effects reported for this organelle (Damiani et al., 2018; Huang et al., 2021; Ichikawa et al., 2014; Rossato et al., 2013; Yu et al., 2020; Zhang et al., 2012). Indeed, we shown that several proteins were downregulated herein after clinically relevant cumulative doses of DOX or MTX and, to our knowledge, this is the first time that MTX-induced cardiotoxicity has been explored in mouse hearts by a proteomic approach (Figure 7).

Indeed, DOX and MTX downregulated several OXPHOS proteins in the enriched mitochondrial fractions, namely ATPA and ATPB from complex V, NADH dehydrogenase [ubiquinone] 1 alpha subcomplex subunit 10 (NDUFA10) and NADH dehydrogenase [ubiquinone] iron-sulfur protein 2 (NDUFS2) belonging to complex I, and cytochrome b-c1 complex subunit 1 (UQCRC1) from complex III. OXPHOS requires the action of five complexes located in the inner mitochondrial membrane to produce ATP (Papa et al., 2012), and the changes observed in our work are in agreement with other studies where a decrease in enzyme activity and protein expression of some OXPHOS complexes occurred after DOX/MTX treatments (Rossato et al., 2014, 2013; Zhang et al., 2012). The inhibition of OXPHOS may be seen as a direct result of redox cycling, mainly studied in DOX, which compromises, mostly, complexes I and III. Conversely, the interaction of DOX and MTX with Top2 and DNA can lead to nuclear and mitochondrial transcriptome changes, and contribute to the downregulation of OXPHOS (Khiati et al., 2014; Lyu et al., 2007; Zhang et al., 2012). Furthermore, PHB2 was downregulated by DOX and MTX, while prohibitin (PHB) was exclusively downregulated by MTX. Cardiolipin and OXPHOS complexes, as well as Cyt c, can be stabilized by the prohibitin complex, which acts as a mitochondrial chaperone to maintain the integrity of the inner membrane (Strub et al., 2011). Both proteins in this complex have been associated with the mitochondrion

organization process and a previous report observed a decrease in PHB expression in response to DOX (Gratia et al., 2012). Additionally, creatine kinase S-type (CKMT2), which is linked to phosphocreatine biosynthesis, was exclusively downregulated by MTX. A previous study of the group using a higher cumulative dose of MTX did not evidence significant changes in cardiac phosphocreatine (Dores-Sousa et al., 2015). On the other hand, several studies reported an increase in the expression of CKMT2 after DOX treatment (Holmgren et al., 2018; Kumar et al., 2011; Zhao et al., 2014), while in the present work no difference was found in animals treated with DOX. Different models and mainly dosage regimens can be crucial for the different cellular responses described, but a strong impact on key mitochondrial proteins is evident, primarily for MTX.

DOX and MTX downregulated mitochondrial fatty acid oxidation pathway proteins, including ETFDH, VLCAD and HADHB. Moreover, carnitine O-palmitoyltransferase 2 (CPT2), electron transfer flavoprotein subunit alpha (ETFA) and medium- and short-chain specific acyl-CoA dehydrogenases (MCAD and SCAD, respectively) were downregulated by MTX. CPT2 is one of the proteins responsible for the transport of long-chain fatty acids across the mitochondrial membrane (Wanders et al., 2010). Oxidation of fatty acids is the main energetic process for ATP production in cardiac tissue (Doenst et al., 2013). VLCAD, MCAD and SCAD, differing on chain lengths substrate specificity, catalyze the first step of the oxidation cycle (Wanders et al., 2010). Reoxidation of these flavoproteins is possible by ETFDH, which accepts electrons from ETF and transfers them to ubiquinone (CoQ) from OXPHOS (Zhang et al., 2006). On the other hand, HADHB is responsible for the last step in the oxidation of long-chain fatty acids, leading to the production of acetyl-CoA (Wanders et al., 2010). Our study shows that these pathways are affected, in several ways, by the two anticancer drugs. Indeed, the decreased amounts of the proteins associated to fatty acids oxidation, most of them acting on the first crucial step of the cycle, led to accumulation of fatty acids and their corresponding acyl-CoA esters inside the cells, in particular on mitochondria. Therefore, the alterations on these proteins disturb the fatty acid dependent-oxidative normal cardiac metabolism. Some studies have reported a downregulation of fatty acid oxidation and a consequent upregulation of glycolysis by DOX (Carvalho et al., 2010; Gratia et al., 2012; Kumar et al., 2011; Yoon et al., 2018). In fact, rats treated with DOX showed a shift from the oxidation of fatty acids, particularly of long-chain fatty acids, to increased oxidation of glucose, along with the inhibition of OXPHOS activity (Carvalho et al., 2010). This change may be related to inhibition of AMP-activated protein kinase (AMPK), which plays a key role in the regulation of energetic metabolism (Gratia et al., 2012; Kumar et al., 2011), and whose inhibition can decrease the metabolization of fatty acids. Herein,

we have demonstrated that MTX also induces downregulation of the fatty oxidation metabolic process, which has never been described before.

DOX and MTX also downregulated proteins related to the tricarboxylic acid cycle, namely SUCLA2 and IDH3A. Furthermore, MTX strongly downregulated CS, MDH2, 2-oxoglutarate dehydrogenase (OGDH) and succinate-CoA ligase [ADP/GDP- and GDP-forming] subunit alpha (SUCLG1 and SUCLG2). While the tricarboxylic acid cycle is the final oxidative pathway for acetyl-CoA produced by carbohydrates, fatty acids, and amino acids, it also provides precursors for many biosynthetic routes. The first step of the tricarboxylic acid cycle is catalyzed by CS, while IDH3A is the subunit of isocitrate dehydrogenase responsible for the decarboxylation of isocitrate to α-ketoglutarate, which is then converted to succinyl-CoA by α-ketoglutarate dehydrogenase complex in which OGDH acts as the E1 component. Succinyl-CoA is converted to succinate by a set of reactions catalyzed by enzymes such as SUCLA2, SUCLG1 and SUCLG2. The last step of the cycle regenerates oxaloacetate from malate and it is catalyzed by MDH2 (Akram, 2014; Melendez-Hevia, 1996). Therefore, it is clear that DOX, but mainly MTX, has an intense impact on several enzymes involved in this cycle. Moreover, the decreased expression of these proteins would result in accumulation of intermediaries of the tricarboxylic acid cycle, such as acetyl-CoA, malate and α-ketoglutarate. These metabolites are essential for other metabolic pathways, thus suggesting that the cardiac metabolism is severely impacted by the two anticancer drugs. In the literature, DOX has been described as affecting many proteins linked to the tricarboxylic acid cycle (Holmgren et al., 2018; Merten et al., 2005; Xi et al., 2011; Yoon et al., 2018); to our knowledge no data on MTX has yet been described. However, other important pathways were disrupted by MTX. PDHA1, dihydrolipoyllysine-residue acetyltransferase component of the pyruvate dehydrogenase complex (DLAT) and dihydrolipoyl dehydrogenase (DLD) belong to the pyruvate dehydrogenase complex, being involved in the biosynthesis of acetyl-CoA, and were severely downregulated by MTX. We found no difference in DOX-treated mice when using a cumulative dose of 9 mg/kg, but changes in DLAT and DLD were linked to DOX either *in vitro* (Yoon et al., 2018) or as *in vivo* models (Zhao et al., 2014) (in the latter with a higher cumulative dose)(Yoon et al., 2018; Zhao et al., 2014). Thus, the decreased expression of these proteins might cause accumulation of pyruvate produced by glycolysis and probably activation of other routes for metabolization of this metabolite such as lactate production.

Administration of MTX led to downregulation of proteins related to amino acid metabolic process, namely aspartate aminotransferase (mAspAT), branched-chain-amino-acid aminotransferase [BCAT(m)] and 3-hydroxyisobutyryl-CoA hydrolase (HIBCH). In the heart, amino acids can either be used as an energy source or used for

biosynthesis processes (Doenst et al., 2013; Wanders et al., 2012). mAspAT is essential for the transamination of L-kynurenine to form kynurenic acid in the catabolism of tryptophan, an aromatic amino acid (Han et al., 2011). The expression of this protein has already been described in other works as altered in response to DOX (Holmgren et al., 2018; Yoon et al., 2018). BCAT(m) catalyzes the first step on the catabolism of branched-chain amino acids, including leucine, isoleucine and valine, while HIBCH is specific for the valine oxidation pathway (Wanders et al., 2012). Additionally, amino acids are transported coupled to intermediates in the tricarboxylic acid cycle by specific carrier proteins (Wanders et al., 2012). OGCP and the calcium-binding mitochondrial carrier protein Aralar1 (SLC25A12) are carrier proteins belonging to the aspartate transmembrane transport and were downregulated by DOX and MTX. SLC25A12 catalyzes the calcium-dependent exchange of cytoplasmic glutamate with mitochondrial aspartate across the mitochondrial membrane. Inside the mitochondria, glutamate can be converted to α-ketoglutarate (Thangaratnarajah et al., 2014). On the other hand, OGCP transports α-ketoglutarate in exchange for malate or other dicarboxylic acids (Gallo et al., 2011). Malate is an intermediate in the tricarboxylic acid cycle that is reversibly converted to oxaloacetate by MDH2 (Melendez-Hevia, 1996), also strongly downregulated by MTX in the present work. Whether these changes resulted in the accumulation of some intermediaries, needs further research.

Likewise, DOX and MTX downregulated PI.VDAC1 along with Mt.VDAC1 and VDAC2. These proteins have been considered to belong to the ion transport process because they allow the diffusion of small molecules across the mitochondrial outer membrane (Hiller et al., 2008). Additionally, VDAC1 may interact with several proteins, including amino acid transporters and antiapoptotic proteins, and VDAC2 plays a critical role in mitochondrial apoptosis (Hiller et al., 2008; Shanmughapriya et al., 2015). Both proteins were also downregulated after DOX in a previous report (Kumar et al., 2011), on conditions that induce apoptosis of cardiomyocytes.

As stated, OGCP was downregulated by both drugs in the heart and in addition to its role in amino acid transport it participates in the process of mitochondrial morphogenesis, which includes mitochondrial fusion and fission events and maintenance of cristae morphology (Gallo et al., 2011). Another protein, MIC60, also linked to this process, was downregulated by both drugs. Indeed, MIC60 is a component of a large protein complex (MICOS) that plays a crucial role in the morphology of the cristae, architecture of the inner membrane, and formation of contact sites with the outer membrane (Ott et al., 2015). MICOS connects to the metaxin-1 and -2 proteins, which belong to the mitochondrial protein translocation apparatus and are essential for the import of proteins into the mitochondria (Armstrong et al., 1999). Metaxin-1 was

previously found downregulated by DOX (Yoon et al., 2018). Our TEM data corroborates the impact of DOX on mitochondrial cristae, possibly through the changes seen in the expression of these proteins. In addition, in a previous work of the group, MTX ultrastructural mitochondrial changes were seen in the cardiac tissue, even 28 days after the last cycle of administration to rats (Rossato et al., 2014).

Additionally, the elongation factor Tu (EFTu) was found downregulated by DOX and MTX. This protein is essential for the regulation of mitochondrial translation (Lei et al., 2012). Changes in its levels were previously reported in DOX (Gratia et al., 2012; Merten et al., 2005). Its downregulation may be associated with the decrease in mitochondrial density observed in total homogenates. Overall, these results highlight the reduction in mitochondrial efficiency, indicated by the decrease in mitochondrial density and the general downregulation of metabolic energy pathways taking place on this organelle after DOX or MTX.

Furthermore, stress-70 protein (HSPA9) and 60 kDa heat shock protein (HSPD1), which were related to the mitochondrial assembly process, were found downregulated by MTX. HSPA9 is a chaperone with an important role in the mitochondrial biogenesis of iron-sulfur cluster and also interacts with the proteins of the MICOS complex, namely MIC60 (Alkhaja et al., 2012). On the other hand, HSPD1 is a chaperonin involved in the importation and folding of mitochondrial proteins, also being crucial for the proper assembly of unfolded polypeptides generated under stress conditions (Viitanen et al., 1992). HSPD1 was previously found downregulated by DOX (Yoon et al., 2018), but not in similar experimental paradigms with multiple cycle administrations and a low cumulative dose (9 mg/kg), as ours.

Western blot analysis of OXPHOS complexes subunits, as well as the enzymatic activities of ATP synthase (complex V) and CS did not show differences among groups, unlike the observed by proteomics. In the latter, several complexes' subunits were downregulated by the drugs in study. Discrepancies between MS-based proteomics and Western blot results were previously reported in mice subjected to DOX therapy, where another protein modification, in that case nitration, was studied (Xi et al., 2011). MS-based proteomics is more sensitive than WB and protein identification might be influenced by protein posttranslational modifications as oxidative and nitrosative modifications (Angel et al., 2012). In fact, UQCRC2, ATPA and ATPB were largely associated with posttranslational oxidative modifications including carbonylation and nitration (Padrão et al., 2011). These modifications have also been reported for ETFDH (Ichihara et al., 2017). Furthermore, while in the literature MTX-induced cardiotoxicity has been much less associated with oxidative dysregulation than DOX, both drugs have been reported to induce oxidative modifications, namely carbonylation or nitration of

proteins (Costa et al., 2020; Dores-Sousa et al., 2015; Xi et al., 2011; Zhao et al., 2014). On the other hand, these same changes may not have a significant impact on the Western blot whose detection depends on the identification of the epitope. Thus, the overall downregulation detected for MS-based proteomics could indicate that affected proteins and biological processes have undoubtedly been altered, but the mechanisms involved were not fully disclosed here. Moreover, the differences between the whole cardiac homogenates and the enriched mitochondrial fractions observed at Western blot level, may advocate for a selection of the least damaged mitochondria during the differential centrifugations undertaken. Damaged mitochondria were possibly discarded during isolation, and a selection among non-ruptured mitochondria was obtained in the methodology used for their isolation (Ascensão et al., 2006). Thus, we observed substantial differences in the selected mitochondria by differential centrifugation, which are probably the healthiest ones. Even so, the supposedly healthier mitochondria reaching the mitochondrial pellet have important proteomic changes after DOX/MTX treatment.

In this study, we also intended to understand the relationship between the effects of the two anticancer drugs and the aging process in the cardiac tissue. Although mitochondrial density decreased similarly in all the three groups, no other link was established. Levels of PGC1α protein were increased in aged control animals, suggesting a compensatory mechanism for the production of new mitochondria to counteract reduced/defective mitochondria. In fact, the aged heart was associated with the overexpression of proteins related to the mitochondrial fission mechanism, which in turn depends on the regulation of PGC1α (Boengler et al., 2017; Ljubicic et al., 2010). Additionally, these animals showed increased levels of MnSOD in whole cardiac muscle extracts indicating a mechanism to prevent the exacerbated levels of ROS that have been found in aged heart (Boengler et al., 2017; Ketul R et al., 2011). MnSOD has been reported as a PGC1α target (Patten et al., 2012). Also consistent with the overexpression of PGC1α, higher levels of ATPB and ETFDH were described here, which are down targets of this key modulator (Scarpulla, 2011). Moreover, aged control animals exhibited increased levels of GAPDH, emphasizing the metabolic shift to glucose oxidation that has been associated with aging of the heart (Ketul R et al., 2011; Tidwell et al., 2017). Thus, aged control animals have demonstrated specific changes related to cardiac mitochondrial dysfunction and related to the aging process (Boengler et al., 2017; Ketul R et al., 2011). Nevertheless, the aged phenotype exhibited a very different pattern of mitochondrial regulation compared to the drugs studied herein.

5. Conclusions

In conclusion, our work showed that DOX and MTX led to a decrease in mitochondrial density, which can lead to the widely reported cardiotoxicity, although none of the drugs shares important impaired pathways with the aged heart. Furthermore, both drugs, DOX and MTX, modulate the mitochondrial proteome and disrupt several important processes that take place on this organelle (Figure 7). Indeed, specific metabolic processes have been affected in different ways, enlightening some future perspectives with possible clinical utility.

Conflict of interest: None

Acknowledgements

This work was supported by national funds by Fundação para a Ciência e a Tecnologia (FCT, Portugal) and co-financed by FEDER and COMPETE for the project "PTDC/DTP-FTO/1489/2014 – POCI-01-0145-FEDER-016537" and the QOPNA/LAQV-REQUIMTE and the Applied Molecular Biosciences Unit - UCIBIO research units (UID/QUI/00062/2019, UIDB/50006/2020 and UIDB/04378/2020). SRB, ARM and VMC acknowledge FCT and European Social Fund for their grants (SFRH/BD/138202/2018, SFRH/BD/129359/2017 and SFRH/BPD/110001/2015) and VMC's grant is funded by FCT, I.P., under the Norma Transitória – DL57/2016/CP1334/CT0006.

References

Akram, M., 2014. Citric Acid Cycle and Role of its Intermediates in Metabolism. Cell Biochem. Biophys. 68, 475–478. https://doi.org/10.1007/s12013-013-9750-1

Alkhaja, A.K., Jans, D.C., Nikolov, M., Vukotic, M., Lytovchenko, O., Ludewig, F., Schliebs, W., Riedel, D., Urlaub, H., Jakobs, S., Deckers, M., 2012. MINOS1 is a conserved component of mitofilin complexes and required for mitochondrial function and cristae organization. Mol. Biol. Cell 23, 247–257. https://doi.org/10.1091/mbc.e11-09-0774

Angel, T.E., Aryal, U.K., Hengel, S.M., Baker, E.S., Kelly, R.T., Robinson, E.W., Smith, R.D., 2012. Mass spectrometry-based proteomics: existing capabilities and future directions. Chem. Soc. Rev. 41, 3912. https://doi.org/10.1039/c2cs15331a

Armstrong, G.T., Ross, J.D., 2014. Late cardiotoxicity in aging adult survivors of childhood cancer. Prog. Pediatr. Cardiol. 36, 19–26. https://doi.org/10.1016/j.ppedcard.2014.09.003

Armstrong, L.C., Saenz, A.J., Bornstein, P., 1999. Metaxin 1 interacts with metaxin 2, a novel related protein associated with the mammalian mitochondrial outer membrane 74, 11–22.

Ascensão, A., Magalhães, J., Soares, J.M.C., Ferreira, R., Neuparth, M.J., Marques, F., Oliveira, P.J., Duarte, J.A., 2006. Endurance training limits the functional alterations of heart rat mitochondria submitted to in vitro anoxia-reoxygenation. Int. J. Cardiol. 109, 169–178. https://doi.org/10.1016/j.ijcard.2005.06.003

Ashley, N., Poulton, J., 2009. Mitochondrial DNA is a direct target of anti-cancer anthracycline drugs. Biochem. Biophys. Res. Commun. 378, 450–455. https://doi.org/10.1016/j.bbrc.2008.11.059

Ayyadevara, S., Mercanti, F., Wang, X., Mackintosh, S.G., Tackett, A.J., Prayaga, S.V.S., Romeo, F., Shmookler Reis, R.J., Mehta, J.L., 2016. Age- and Hypertension-Associated Protein Aggregates in Mouse Heart Have Similar Proteomic Profiles. Hypertension 67, 1006–1013. https://doi.org/10.1161/HYPERTENSIONAHA.115.06849

Boengler, K., Kosiol, M., Mayr, M., Schulz, R., Rohrbach, S., 2017. Mitochondria and ageing: role in heart, skeletal muscle and adipose tissue: Mitochondria and ageing. J. Cachexia Sarcopenia Muscle 8, 349–369. https://doi.org/10.1002/jcsm.12178

Calvo, S.E., Clauser, K.R., Mootha, V.K., 2016. MitoCarta2.0: an updated inventory of mammalian mitochondrial proteins. Nucleic Acids Res. 44, D1251–D1257. https://doi.org/10.1093/nar/gkv1003

Carvalho, R.A., Sousa, R.P.B., Cadete, V.J.J., Lopaschuk, G.D., Palmeira, C.M.M., Bjork, J.A., Wallace, K.B., 2010. Metabolic remodeling associated with subchronic doxorubicin cardiomyopathy. Toxicology 270, 92–98. https://doi.org/10.1016/j.tox.2010.01.019

Chen, Y., Daosukho, C., Opii, W.O., Turner, D.M., Pierce, W.M., Klein, J.B., Vore, M., Butterfield, D.A., St. Clair, D.K., 2006. Redox proteomic identification of oxidized cardiac proteins in Adriamycin-treated mice. Free Radic. Biol. Med. 41, 1470–1477. https://doi.org/10.1016/j.freeradbiomed.2006.08.006

Chung, I.Y., Lee, J.W., Moon, H.-G., Shin, K.H., Han, W., Son, B.H., Ahn, S.-H., Noh, D.-Y., 2020. Effect of standard low-dose anthracycline chemotherapy on late congestive heart failure in breast cancer survivors aged between 50 and 59 at diagnosis: A nationwide study. The Breast 53, 125–129. https://doi.org/10.1016/j.breast.2020.07.006

Citron, M.L., Berry, D.A., Cirrincione, C., Hudis, C., Winer, E.P., Gradishar, W.J., Davidson, N.E., Martino, S., Livingston, R., Ingle, J.N., Perez, E.A., Carpenter, J., Hurd, D., Holland, J.F., Smith, B.L., Sartor, C.I., Leung, E.H., Abrams, J., Schilsky, R.L., Muss, H.B., Norton, L., 2003. Randomized Trial of Dose-Dense Versus Conventionally Scheduled and Sequential Versus Concurrent

Combination Chemotherapy as Postoperative Adjuvant Treatment of Node-Positive Primary Breast Cancer: First Report of Intergroup Trial C9741/Cancer and Leukemia Group B Trial 9741. J. Clin. Oncol. 21, 1431–1439. https://doi.org/10.1200/JCO.2003.09.081

Coore, H.G., Denton, R.M., Martin, B.R., Randle, P.J., 1971. Regulation of adipose tissue pyruvate dehydrogenase by insulin and other hormones. Biochem. J. 125, 115–127. https://doi.org/10.1042/bj1250115

Costa, V.M., Capela, J.P., Sousa, J.R., Eleutério, R.P., Rodrigues, P.R.S., Dores-Sousa, J.L., Carvalho, R.A., Lourdes Bastos, M., Duarte, J.A., Remião, F., Almeida, M.G., Varner, K.J., Carvalho, F., 2020. Mitoxantrone impairs proteasome activity and prompts early energetic and proteomic changes in HL-1 cardiomyocytes at clinically relevant concentrations. Arch. Toxicol. 94, 4067–4084. https://doi.org/10.1007/s00204-020-02874-4

Cui, Y., Piao, C.-S., Ha, K.-C., Kim, D.-S., Lee, G.-H., Kim, H.-K., Chae, S.-W., Lee, Y.-C., Park, S.-J., Yoo, W.-H., Kim, H.-R., Chae, H.-J., 2010. Measuring adriamycin-induced cardiac hemodynamic dysfunction with a proteomics approach. Immunopharmacol. Immunotoxicol. 32, 376–386. https://doi.org/10.3109/08923970903440168

Damiani, R.M., Moura, D.J., Viau, C.M., Brito, V., Morás, A.M., Henriques, J.A.P., Saffi, J., 2018. Influence of PARP-1 inhibition in the cardiotoxicity of the topoisomerase 2 inhibitors doxorubicin and mitoxantrone. Toxicol. In Vitro 52, 203–213. https://doi.org/10.1016/j.tiv.2018.06.013

Davies, K.J., Doroshow, J.H., 1986. Redox cycling of anthracyclines by cardiac mitochondria. I. Anthracycline radical formation by NADH dehydrogenase. J. Biol. Chem. 261, 3060–3067.

Doenst, T., Nguyen, T.D., Abel, E.D., 2013. Cardiac Metabolism in Heart Failure: Implications Beyond ATP Production. Circ. Res. 113, 709–724. https://doi.org/10.1161/CIRCRESAHA.113.300376

Dores-Sousa, J.L., Duarte, J.A., Seabra, V., Bastos, M. de L., Carvalho, F., Costa, V.M., 2015. The age factor for mitoxantrone's cardiotoxicity: Multiple doses render the adult mouse heart more susceptible to injury. Toxicology 329, 106–119. https://doi.org/10.1016/j.tox.2015.01.006

Doroshow, J.H., Davies, K.J., 1986. Redox cycling of anthracyclines by cardiac mitochondria. II. Formation of superoxide anion, hydrogen peroxide, and hydroxyl radical. J. Biol. Chem. 261, 3068–3074.

Dutta, S., Sengupta, P., 2016. Men and mice: Relating their ages. Life Sci. 152, 244–248. https://doi.org/10.1016/j.lfs.2015.10.025

Favreau-Lessard, A.J., Blaszyk, H., Jones, M.A., Sawyer, D.B., Pinz, I.M., 2019. Systemic and cardiac susceptibility of immune compromised mice to doxorubicin. Cardio-Oncol. 5, 2. https://doi.org/10.1186/s40959-019-0037-6

Ferreira, R., Neuparth, M., Nogueira-Ferreira, R., Magalhães, S., Aroso, M., Bovolini, J., Lara Santos, L., Oliveira, P., Vitorino, R., Moreira-Gonçalves, D., 2018. Exercise Training Impacts Cardiac Mitochondrial Proteome Remodeling in Murine Urothelial Carcinoma. Int. J. Mol. Sci. 20, 127. https://doi.org/10.3390/ijms20010127

Ferreira, R., Vitorino, R., Padrão, A.I., Espadas, G., Mancuso, F.M., Moreira-Gonçalves, D., Castro-Sousa, G., Henriques-Coelho, T., Oliveira, P.A., Barros, A.S., Duarte, J.A., Sabidó, E., Amado, F., 2014. Lifelong Exercise Training Modulates Cardiac Mitochondrial Phosphoproteome in Rats. J. Proteome Res. 13, 2045–2055. https://doi.org/10.1021/pr4011926

Filipa Reis-Mendes, A., Sousa, E., de Lourdes Bastos, M., Marisa Costa, V., 2015. The Role of the Metabolism of Anticancer Drugs in Their Induced-Cardiotoxicity. Curr. Drug Metab. 17, 75–90. https://doi.org/10.2174/1389200216666151103114926

Gallo, M., Park, D., Luciani, D.S., Kida, K., Palmieri, F., Johnson, J.D., Riddle, D.L., 2011. MISC-1/OGC Links Mitochondrial Metabolism, Apoptosis and Insulin Secretion. PLoS ONE 6, 13.

Gratia, S., Kay, L., Michelland, S., Sève, M., Schlattner, U., Tokarska-Schlattner, M., 2012. Cardiac phosphoproteome reveals cell signaling events involved in doxorubicin cardiotoxicity. J. Proteomics 75, 4705–4716. https://doi.org/10.1016/j.jprot.2012.02.004

Han, Q., Robinson, H., Cai, T., Tagle, D.A., Li, J., 2011. Biochemical and structural characterization of mouse mitochondrial aspartate aminotransferase, a newly identified kynurenine aminotransferase-IV. Biosci. Rep. 31, 323–332. https://doi.org/10.1042/BSR20100117

Hao, E., Mukhopadhyay, P., Cao, Z., Erdélyi, K., Holovac, E., Liaudet, L., Lee, W.-S., Haskó, G., Mechoulam, R., Pacher, P., 2015. Cannabidiol Protects against Doxorubicin-Induced Cardiomyopathy by Modulating Mitochondrial Function and Biogenesis. Mol. Med. 21, 38–45. https://doi.org/10.2119/molmed.2014.00261

Hiller, S., Garces, R.G., Malia, T.J., Orekhov, V.Y., Colombini, M., Wagner, G., 2008. Solution Structure of the Integral Human Membrane Protein VDAC-1 in Detergent Micelles. Science 321, 1206–1210. https://doi.org/10.1126/science.1161302

Hixon, S.C., Ellis, C.N., Daugherty, J.P., 1981. Heart mitochondrial DNA synthesis: Preferential inhibition by adriamycin. J. Mol. Cell. Cardiol. 13, 855–860. https://doi.org/10.1016/0022-2828(81)90242-X

Holmgren, G., Sartipy, P., Andersson, C.X., Lindahl, A., Synnergren, J., 2018. Expression Profiling of Human Pluripotent Stem Cell-Derived Cardiomyocytes Exposed to Doxorubicin—Integration and Visualization of Multi-Omics Data. Toxicol. Sci. 163, 182–195. https://doi.org/10.1093/toxsci/kfy012

Huang, C., Zhang, X., Ramil, J.M., Rikka, S., Kim, L., Lee, Y., Gude, N.A., Thistlethwaite, P.A., Sussman, M.A., Gottlieb, R.A., Gustafsson, Å.B., 2010. Juvenile Exposure to Anthracyclines Impairs Cardiac Progenitor Cell Function and Vascularization Resulting in Greater Susceptibility to Stress-Induced Myocardial Injury in Adult Mice. Circulation 121, 675–683. https://doi.org/10.1161/CIRCULATIONAHA.109.902221

Huang, W.-P., Yin, W.-H., Chen, J.-S., Huang, P.-H., Chen, J.-W., Lin, S.-J., 2021. Fenofibrate attenuates doxorubicin-induced cardiac dysfunction in mice via activating the eNOS/EPC pathway. Sci. Rep. 11, 1159. https://doi.org/10.1038/s41598-021-80984-4

Ichihara, S., Suzuki, Y., Chang, J., Kuzuya, K., Inoue, C., Kitamura, Y., Oikawa, S., 2017. Involvement of oxidative modification of proteins related to ATP synthesis in the left ventricles of hamsters with cardiomyopathy. Sci. Rep. 7, 9243. https://doi.org/10.1038/s41598-017-08546-1

Ichikawa, Y., Ghanefar, M., Bayeva, M., Wu, R., Khechaduri, A., Prasad, S.V.N., Mutharasan, R.K., Naik, T.J., Ardehali, H., 2014. Cardiotoxicity of doxorubicin is mediated through mitochondrial iron accumulation. J. Clin. Invest. 124, 617–630. https://doi.org/10.1172/JCI72931

Jain, D., Aronow, W., 2019. Cardiotoxicity of cancer chemotherapy in clinical practice. Hosp. Pract. 47, 6–15. https://doi.org/10.1080/21548331.2018.1530831

Jordan, J.H., Castellino, S.M., Meléndez, G.C., Klepin, H.D., Ellis, L.R., Lamar, Z., Vasu, S., Kitzman, D.W., Ntim, W.O., Brubaker, P.H., Reichek, N., D'Agostino, R.B., Hundley, W.G., 2019. Left Ventricular Mass Change After Anthracycline Chemotherapy 11, 18.

Karpievitch, Y.V., Nikolic, S.B., Wilson, R., Sharman, J.E., Edwards, L.M., 2014. Metabolomics Data Normalization with EigenMS. PLoS ONE 9, e116221. https://doi.org/10.1371/journal.pone.0116221

Kassambara, A., Mundt, F., 2020. Extract and Visualize the Results of Multivariate Data Analyses.

Ketul R, C., Haitham, E.-S., John M, S., 2011. Mitochondria and the aging heart: Mitochondria and the aging heart. J. Geriatr. Cardiol. 8, 159–167. https://doi.org/10.3724/SP.J.1263.2011.00159

Khiati, S., Dalla Rosa, I., Sourbier, C., Ma, X., Rao, V.A., Neckers, L.M., Zhang, H., Pommier, Y., 2014. Mitochondrial Topoisomerase I (Top1mt) Is a Novel Limiting Factor of Doxorubicin Cardiotoxicity. Clin. Cancer Res. 20, 4873–4881. https://doi.org/10.1158/1078-0432.CCR-13-3373

Kolde, R., 2019. Pretty Heatmaps.

Kumar, S.N., 2011. Analysis of proteome changes in doxorubicin-treated adult rat cardiomyocyte. J. PROTEOMICS 15.

Kumar, S.N., Konorev, E.A., Aggarwal, D., Kalyanaraman, B., 2011. Analysis of proteome changes in doxorubicin-treated adult rat cardiomyocyte. J. Proteomics 74, 683–697. https://doi.org/10.1016/j.jprot.2011.02.013

Laemmli, U.K., 1970. Cleavage of structural proteins during the assembly of the head of bacteriophage T4. Nature 227, 680–685.

Larsen, S., Nielsen, J., Hansen, C.N., Nielsen, L.B., Wibrand, F., Stride, N., Schroder, H.D., Boushel, R., Helge, J.W., Dela, F., Hey-Mogensen, M., 2012. Biomarkers of mitochondrial content in skeletal muscle of healthy young human subjects: Biomarkers of mitochondrial content. J. Physiol. 590, 3349–3360. https://doi.org/10.1113/jphysiol.2012.230185

Lê, S., Josse, J., Husson, F., 2008. FactoMineR: An R Package for Multivariate Analysis. J. Stat. Softw. 25. https://doi.org/10.18637/jss.v025.i01

Lebrecht, D., Setzer, B., Ketelsen, U.-P., Haberstroh, J., Walker, U.A., 2003. Time-dependent and tissue-specific accumulation of mtDNA and respiratory chain defects in chronic doxorubicin cardiomyopathy. Circulation 108, 2423–2429. https://doi.org/10.1161/01.CIR.0000093196.59829.DF

Lei, Y., Wen, H., Yu, Y., Taxman, D.J., Zhang, L., Widman, D.G., Swanson, K.V., Wen, K.-W., Damania, B., Moore, C.B., Giguère, P.M., Siderovski, D.P., Hiscott, J., Razani, B., Semenkovich, C.F., Chen, X., Ting, J.P.-Y., 2012. The Mitochondrial Proteins NLRX1 and TUFM Form a Complex that Regulates Type I Interferon and Autophagy. Immunity 36, 933–946. https://doi.org/10.1016/j.immuni.2012.03.025

Ljubicic, V., Menzies, K.J., Hood, D.A., 2010. Mitochondrial dysfunction is associated with a pro-apoptotic cellular environment in senescent cardiac muscle. Mech. Ageing Dev. 131, 79–88. https://doi.org/10.1016/j.mad.2009.12.004

Low, R.L., Orton, S., Friedman, D.B., 2003. A truncated form of DNA topoisomerase IIβ associates with the mtDNA genome in mammalian mitochondria: DNA Topo IIβ mammalian mtDNA. Eur. J. Biochem. 270, 4173–4186. https://doi.org/10.1046/j.1432-1033.2003.03814.x

Löwenberg, B., Suciu, S., Archimbaud, E., Haak, H., Stryckmans, P., de Cataldo, R., Dekker, A.W., Berneman, Z.N., Thyss, A., van der Lelie, J., Sonneveld, P., Visani, G., Fillet, G., Hayat, M., Hagemeijer, A., Solbu, G., Zittoun, R., 1998. Mitoxantrone versus daunorubicin in induction-consolidation chemotherapy--the value of low-dose cytarabine for maintenance of remission, and an assessment of prognostic factors in acute myeloid leukemia in the elderly: final report. European Organization for the Research and Treatment of Cancer and the Dutch-Belgian Hemato-Oncology Cooperative Hovon Group. J. Clin. Oncol. 16, 872–881. https://doi.org/10.1200/JCO.1998.16.3.872

Lyu, Y.L., Kerrigan, J.E., Lin, C.-P., Azarova, A.M., Tsai, Y.-C., Ban, Y., Liu, L.F., 2007. Topoisomerase II Mediated DNA Double-Strand Breaks: Implications in Doxorubicin Cardiotoxicity and Prevention by Dexrazoxane. Cancer Res. 67, 8839–8846. https://doi.org/10.1158/0008-5472.CAN-07-1649

Melendez-Hevia, E. et al, 1996. The Puzzle of the Krebs Citric Acid Cycle: Assembling the Pieces of Chemically Feasible Reactions, and Opportunism in the Design of Metabolic Pathways During Evolution 43, 293–303.

Merten, K.E., Feng, W., Zhang, L., Pierce, W., Cai, J., Klein, J.B., Kang, Y.J., 2005. Modulation of Cytochrome c Oxidase-Va Is Possibly Involved in Metallothionein Protection from Doxorubicin Cardiotoxicity. J. Pharmacol. Exp. Ther. 315, 1314–1319. https://doi.org/10.1124/jpet.105.089763

Ott, C., Dorsch, E., Fraunholz, M., Straub, S., Kozjak-Pavlovic, V., 2015. Detailed Analysis of the Human Mitochondrial Contact Site Complex Indicate a Hierarchy of Subunits. PLOS ONE 10, e0120213. https://doi.org/10.1371/journal.pone.0120213

Padrão, A.I., Ferreira, R.M.P., Vitorino, R., Alves, R.M.P., Neuparth, M.J., Duarte, J.A., Amado, F., 2011. OXPHOS susceptibility to oxidative modifications: The role of heart mitochondrial subcellular location. Biochim. Biophys. Acta BBA - Bioenerg. 1807, 1106–1113. https://doi.org/10.1016/j.bbabio.2011.04.002

Papa, S., Martino, P.L., Capitanio, G., Gaballo, A., De Rasmo, D., Signorile, A., Petruzzella, V., 2012. The Oxidative Phosphorylation System in Mammalian Mitochondria, in: Scatena, R., Bottoni, P., Giardina, B. (Eds.), Advances in Mitochondrial Medicine, Advances in Experimental Medicine and Biology. Springer Netherlands, Dordrecht, pp. 3–37. https://doi.org/10.1007/978-94-007-2869-1_1

Patten, I.S., Rana, S., Shahul, S., Rowe, G.C., Jang, C., Liu, L., Hacker, M.R., Rhee, J.S., Mitchell, J., Mahmood, F., Hess, P., Farrell, C., Koulisis, N., Khankin, E.V., Burke, S.D., Tudorache, I., Bauersachs, J., Monte, F. del, Hilfiker-Kleiner, D., Karumanchi, S.A., Arany, Z., 2012. Cardiac angiogenic imbalance leads to peripartum cardiomyopathy. Nature 485, 333–338. https://doi.org/10.1038/nature11040

Pereira, G.C., Pereira, S.P., Tavares, L.C., Carvalho, F.S., Magalhães-Novais, S., Barbosa, I.A., Santos, M.S., Bjork, J., Moreno, A.J., Wallace, K.B., Oliveira, P.J., 2016. Cardiac cytochrome c and cardiolipin depletion during anthracycline-induced chronic depression of mitochondrial function. Mitochondrion 30, 95–104. https://doi.org/10.1016/j.mito.2016.07.005

Reagan-Shaw, S., Nihal, M., Ahmad, N., 2008. Dose translation from animal to human studies revisited. FASEB J. 22, 659–661. https://doi.org/10.1096/fj.07-9574LSF

Reis, A., Dores, J.L., Padrão, A.I., Duarte, M., Duarte, J.A., Seabra, V., Gonçalves, S., Remião, F., Carvalho, F., Sousa, E., Bastos, M.L., Costa, V.M., 2021. Inflammation as a Possible Trigger for Mitoxantrone-Induced Cardiotoxicity: An In Vivo Study in Adult and Infant Mice 28.

Rossato, L.G., Costa, V.M., Dallegrave, E., Arbo, M., Silva, R., Ferreira, R., Amado, F., Dinis-Oliveira, R.J., Duarte, J.A., de Lourdes Bastos, M., Palmeira, C., Remião, F., 2014. Mitochondrial Cumulative Damage Induced by Mitoxantrone: Late Onset Cardiac Energetic Impairment. Cardiovasc. Toxicol. 14, 30–40. https://doi.org/10.1007/s12012-013-9230-2

Rossato, L.G., Costa, V.M., Vilas-Boas, V., de Lourdes Bastos, M., Rolo, A., Palmeira, C., Remião, F., 2013. Therapeutic Concentrations of Mitoxantrone Elicit Energetic Imbalance in H9c2 Cells as an Earlier Event. Cardiovasc. Toxicol. 13, 413–425. https://doi.org/10.1007/s12012-013-9224-0

Scarpulla, R.C., 2011. Metabolic control of mitochondrial biogenesis through the PGC-1 family regulatory network. Biochim. Biophys. Acta BBA - Mol. Cell Res. 1813, 1269–1278. https://doi.org/10.1016/j.bbamcr.2010.09.019

Shanmughapriya, S., Rajan, S., Hoffman, N.E., Higgins, A.M., Tomar, D., Nemani, N., Hines, K.J., Smith, D.J., Eguchi, A., Vallem, S., Shaikh, F., Cheung, M., Leonard, N.J., Stolakis, R.S., Wolfers, M.P., Ibetti, J., Chuprun, J.K., Jog, N.R., Houser, S.R., Koch, W.J., Elrod, J.W., Madesh, M., 2015. SPG7 Is an Essential and Conserved Component of the Mitochondrial Permeability Transition Pore. Mol. Cell 60, 47–62. https://doi.org/10.1016/j.molcel.2015.08.009

Shevchenko, A., Tomas, H., Havli, J., Olsen, J.V., Mann, M., 2006. In-gel digestion for mass spectrometric characterization of proteins and proteomes. Nat. Protoc. 1, 2856–2860. https://doi.org/10.1038/nprot.2006.468

Siegel, R.L., Miller, K.D., Jemal, A., 2019. Cancer statistics, 2019. CA. Cancer J. Clin. 69, 7–34. https://doi.org/10.3322/caac.21551

Simon, N., Papa, K., Vidal, J., Boulamery, A., Bruguerolle, B., 2003. Circadian Rhythms of Oxidative Phosphorylation: Effects of Rotenone and Melatonin on Isolated Rat Brain Mitochondria. Chronobiol. Int. 20, 451–461. https://doi.org/10.1081/CBI-120021385

Stauch, K.L., Purnell, P.R., Villeneuve, L.M., Fox, H.S., 2015. Proteomic analysis and functional characterization of mouse brain mitochondria during aging reveal alterations in energy metabolism. PROTEOMICS 15, 1574–1586. https://doi.org/10.1002/pmic.201400277

Strub, G.M., Paillard, M., Liang, J., Gomez, L., Allegood, J.C., Hait, N.C., Maceyka, M., Price, M.M., Chen, Q., Simpson, D.C., Kordula, T., Milstien, S., Lesnefsky, E.J., Spiegel, S., 2011. Sphingosine-1-phosphate produced by sphingosine kinase 2 in mitochondria interacts with prohibitin 2 to regulate complex IV assembly and respiration. FASEB J. 25, 600–612. https://doi.org/10.1096/fj.10-167502

Sun, N., Youle, R.J., Finkel, T., 2016. The Mitochondrial Basis of Aging. Mol. Cell 61, 654–666. https://doi.org/10.1016/j.molcel.2016.01.028

Taylor, S.W., Fahy, E., Zhang, B., Glenn, G.M., Warnock, D.E., Wiley, S., Murphy, A.N., Gaucher, S.P., Capaldi, R.A., Gibson, B.W., Ghosh, S.S., 2003. Characterization of the human heart mitochondrial proteome. Nat. Biotechnol. 21, 281–286. https://doi.org/10.1038/nbt793

Thangaratnarajah, C., Ruprecht, J.J., Kunji, E.R.S., 2014. Calcium-induced conformational changes of the regulatory domain of human mitochondrial aspartate/glutamate carriers. Nat. Commun. 5, 5491. https://doi.org/10.1038/ncomms6491

Tidwell, T.R., Søreide, K., Hagland, H.R., 2017. Aging, Metabolism, and Cancer Development: from Peto's Paradox to the Warburg Effect. Aging Dis. 8, 662–676. https://doi.org/10.14336/AD.2017.0713

Varga, Z.V., Ferdinandy, P., Liaudet, L., Pacher, P., 2015. Drug-induced mitochondrial dysfunction and cardiotoxicity. Am. J. Physiol.-Heart Circ. Physiol. 309, H1453–H1467. https://doi.org/10.1152/ajpheart.00554.2015

Vedam, K., Nishijima, Y., Druhan, L.J., Khan, M., Moldovan, N.I., Zweier, J.L., Ilangovan, G., 2010. Role of heat shock factor-1 activation in the doxorubicin-induced heart failure in mice. Am. J. Physiol.-Heart Circ. Physiol. 298, H1832–H1841. https://doi.org/10.1152/ajpheart.01047.2009

Vejpongsa, P., Yeh, E.T.H., 2013. Topoisomerase 2β: A Promising Molecular Target for Primary Prevention of Anthracycline-Induced Cardiotoxicity. Clin. Pharmacol. Ther. 95, 45–52. https://doi.org/10.1038/clpt.2013.201

Viitanen, P.V., Lorimer, G.H., Seetharam, R., Gupta, R.S., Oppenheim, J., Thomas, J.O., Cowan, N.J., 1992. Mammalian mitochondrial chaperonin 60 functions as a single toroidal ring. J. Biol. Chem. 267, 695–698.

Wanders, R.J.A., Duran, M., Loupatty, F.J., 2012. Enzymology of the branched-chain amino acid oxidation disorders: the valine pathway. J. Inherit. Metab. Dis. 35, 5–12. https://doi.org/10.1007/s10545-010-9236-x

Wanders, R.J.A., Ruiter, J.P.N., IJlst, L., Waterham, H.R., Houten, S.M., 2010. The enzymology of mitochondrial fatty acid beta-oxidation and its application to follow-up analysis of positive neonatal screening results. J. Inherit. Metab. Dis. 33, 479–494. https://doi.org/10.1007/s10545-010-9104-8

Wickham, H., 2009. ggplot2: Elegant Graphics for Data Analysis, Use R! Springer-Verlag, New York. https://doi.org/10.1007/978-0-387-98141-3

Willis, M.S., Parry, T.L., Brown, D.I., Mota, R.I., Huang, W., Beak, J.Y., Sola, M., Zhou, C., Hicks, S.T., Caughey, M.C., D'Agostino, R.B., Jordan, J., Hundley, W.G.,

Jensen, B.C., 2019. Doxorubicin Exposure Causes Subacute Cardiac Atrophy Dependent on the Striated Muscle–Specific Ubiquitin Ligase MuRF1. Circ. Heart Fail. 12, e005234. https://doi.org/10.1161/CIRCHEARTFAILURE.118.005234

Xi, L., Zhu, S.-G., Hobbs, D.C., Kukreja, R.C., 2011. Identification of protein targets underlying dietary nitrate-induced protection against doxorubicin cardiotoxicity. J. Cell. Mol. Med. 15, 2512–2524. https://doi.org/10.1111/j.1582-4934.2011.01257.x

Xu, Z.-M., Li, C.-B., Liu, Q.-L., Li, P., Yang, H., 2018. Ginsenoside Rg1 Prevents Doxorubicin-Induced Cardiotoxicity through the Inhibition of Autophagy and Endoplasmic Reticulum Stress in Mice. Int. J. Mol. Sci. 19, 3658. https://doi.org/10.3390/ijms19113658

Yang, Y., Zhang, H., Li, X., Yang, T., Jiang, Q., 2014. Effects of PPARα/PGC-1α on the myocardial energy metabolism during heart failure in the doxorubicin induced dilated cardiomyopathy in mice 7, 2435–2442.

Ye, X., Zhou, X.-J., Zhang, H., 2018. Exploring the Role of Autophagy-Related Gene 5 (ATG5) Yields Important Insights Into Autophagy in Autoimmune/Autoinflammatory Diseases. Front. Immunol. 9, 2334. https://doi.org/10.3389/fimmu.2018.02334

Yoon, C., Kim, H., Mishchenko, N., Vasileva, E., Fedoreyev, S., Stonik, V., Han, J., 2018. Spinochrome D Attenuates Doxorubicin-Induced Cardiomyocyte Death via Improving Glutathione Metabolism and Attenuating Oxidative Stress. Mar. Drugs 17, 2. https://doi.org/10.3390/md17010002

Yu, X., Ruan, Y., Shen, T., Qiu, Q., Yan, M., Sun, S., Dou, L., Huang, X., Wang, Q., Zhang, X., Man, Y., Tang, W., Jin, Z., Li, J., 2020. Dexrazoxane Protects Cardiomyocyte from Doxorubicin-Induced Apoptosis by Modulating miR-17-5p. BioMed Res. Int. 2020, 1–11. https://doi.org/10.1155/2020/5107193

Zhang, J., Frerman, F.E., Kim, J.-J.P., 2006. Structure of electron transfer flavoprotein-ubiquinone oxidoreductase and electron transfer to the mitochondrial ubiquinone pool. Proc. Natl. Acad. Sci. 103, 16212–16217. https://doi.org/10.1073/pnas.0604567103

Zhang, L., Liu, L., Li, X., 2020. MiR-526b-3p mediates doxorubicin-induced cardiotoxicity by targeting STAT3 to inactivate VEGFA. Biomed. Pharmacother. 123, 109751. https://doi.org/10.1016/j.biopha.2019.109751

Zhang, S., Liu, X., Bawa-Khalfe, T., Lu, L.-S., Lyu, Y.L., Liu, L.F., Yeh, E.T.H., 2012. Identification of the molecular basis of doxorubicin-induced cardiotoxicity. Nat. Med. 18, 1639–1642. https://doi.org/10.1038/nm.2919

Zhao, Y., Miriyala, S., Miao, L., Mitov, M., Schnell, D., Dhar, S.K., Cai, J., Klein, J.B., Sultana, R., Butterfield, D.A., Vore, M., Batinic-Haberle, I., Bondada, S., St. Clair, D.K., 2014. Redox proteomic identification of HNE-bound mitochondrial proteins in cardiac tissues reveals a systemic effect on energy metabolism after doxorubicin treatment. Free Radic. Biol. Med. 72, 55–65. https://doi.org/10.1016/j.freeradbiomed.2014.03.001

Table and Figure legends

Table legends

Table 1. Whole-body weight (g), heart weight (g), brain weight (g), heart weight-to-brain weight ratio, heart weight-to-whole body weight (mg/g) at sacrifice, and heart mitochondrial isolation yield (mg protein/g tissue and mtDNA-to-tDNA) of young control, aged control, young DOX and young MTX animals.

Values are expressed as mean ± SD (n = 7-9 for young control; n = 5-6 for aged control; n = 8-9 for young DOX and young MTX). The statistical analyses were done by ordinary one-way ANOVA followed by Tukey's multiple comparisons (* $p<0.05$ vs. young control, ** $p<0.01$ vs. young control, *** $p<0.001$ vs. young control, $^{+}$ $p<0.05$ vs. aged control, $^{++}$ $p<0.01$ vs. aged control, $^{+++}$ $p<0.001$ vs. aged control, $^{++++}$ $p<0.0001$ vs. aged control).

Figure legends

Figure 1. Citrate synthase (CS) activity measured spectrophotometrically, and peroxisome proliferator-activated receptor γ coactivator 1 α (PGC1α), autophagy protein 5 (ATG5) and manganese superoxide dismutase (MnSOD) expression evaluated by Western blotting on whole cardiac homogenates of young control, aged control, young DOX and young MTX animals. PGC1α, ATG5 and MnSOD content is presented after normalization to total protein with Ponceau S staining, and in percentage of young control group. Representative images of the Western blots and the Ponceau S staining obtained are presented for each protein. The PGC1α-to-CS activity ratio is also presented. Values are expressed as mean ± SD (n = 7 for young control, young DOX and young MTX of CS activity; n = 5 for aged control of CS activity; n = 4-6 for PGC1α, PGC1α-to-CS activity, ATG5 and MnSOD). The statistical analyzes were done by ordinary one-way ANOVA followed by Tukey's multiple comparisons (* $p<0.05$, ** $p<0.01$, *** $p<0.001$, **** $p<0.0001$).

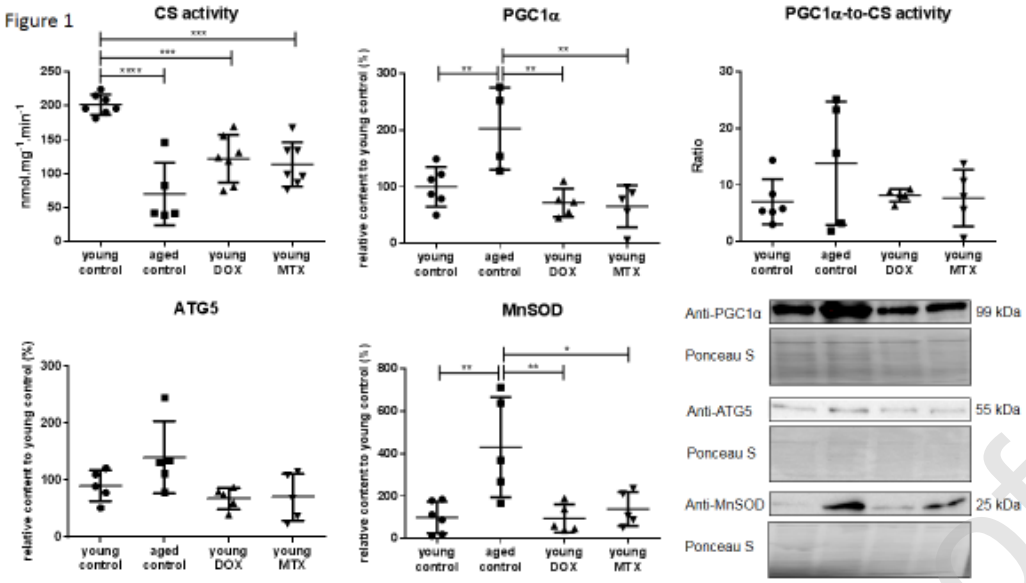

Figure 2. Representative electron micrographs from the young control (A), young DOX (B), and young MTX (C) animals (n = 3). Contrasting with a normal ultrastructure of mitochondria and cytosolic space depicted in A, it is possible to observe in B a pronounced intracellular edema (arrows) suggested by the enlarged cytosolic space among organelles and myofibrils and prevalent mitochondria with aberrant cristae morphology ($); a widespread mitochondrial swelling (*), a primary lysosome (&), and a lipid droplet (#) are depicted in C.

Figure 2

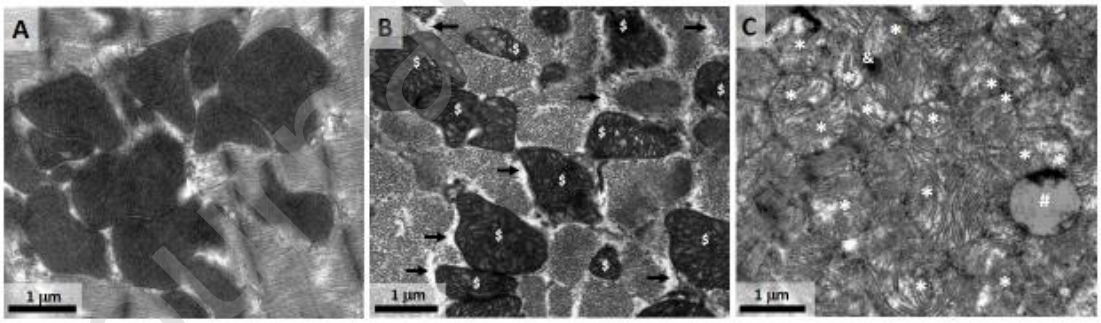

Figure 3. ATP synthase subunit β (ATPB), glyceraldehyde-3-phosphate dehydrogenase (GAPDH) and electron transfer flavoprotein-ubiquinone oxidoreductase (ETFDH) expression evaluated by Western blotting on whole cardiac homogenates of young control, aged control, young DOX and young MTX animals. ATPB, GAPDH and ETFDH

content is presented after normalization to total protein with Ponceau S staining, and in percentage of young control group. Representative images of the Western blots and the Ponceau S staining obtained are presented for each protein. The glycolytic (GAPDH-to-ATPB) and β-oxidation (ETFDH-to-ATPB) ratios are also presented. Values are expressed as mean ± SD (n = 4-6 for ATPB, ETFDH and ETFDH-to-ATPB; n = 3-4 for GAPDH and GAPDH-to-ATPB). The statistical analyzes were done by ordinary one-way ANOVA followed by Tukey's multiple comparisons (* p<0.05, ** p<0.01, *** p<0.001, **** p<0.0001).

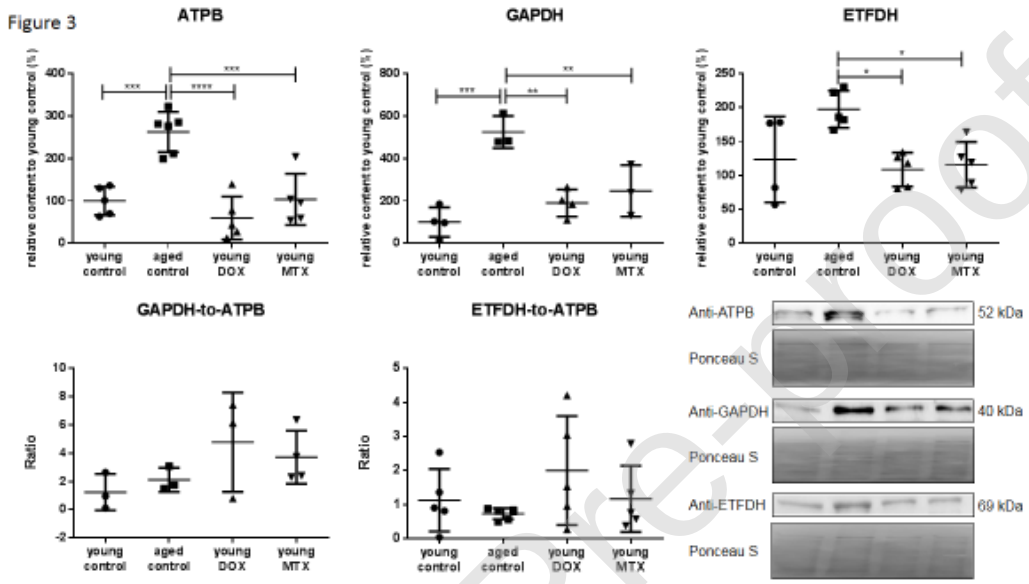

Figure 4. Principal component analysis (PCA) of the proteomics data of mitochondrial enriched fractions of young control (green), aged control (orange), young DOX (purple) and young MTX (pink) animals (n = 4 for young control, young DOX and young MTX; n = 5 for aged control). The shaded areas indicate the 95% confidence ellipse regions for each experimental group.

Figure 4

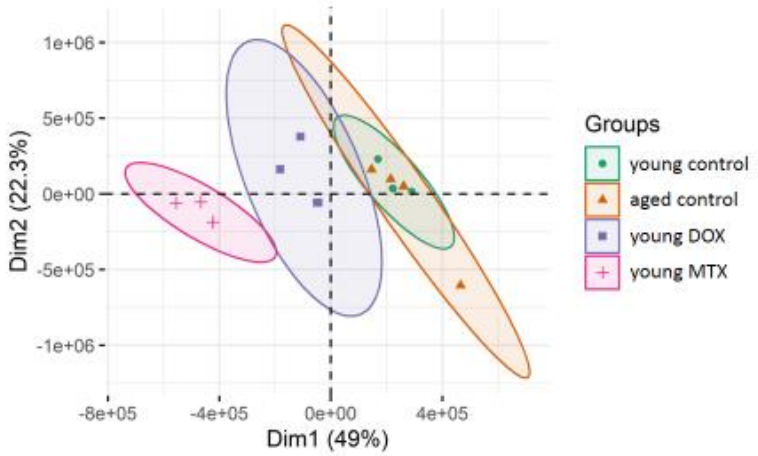

Figure 5. Heatmap and clustering for the top 50 proteins from mitochondrial enriched fractions of young control (green), aged control (orange), young DOX (purple) and young MTX (pink) animals (n = 4 for young control, young DOX and young MTX; n = 5 for aged control). Each column of squares indicates an individual sample, and each row of squares indicates an individual protein profile. Protein expression levels were scaled to row mean. The color key relates the heatmap colors to the standard score (z-score), that is, deviation from the row mean in units of standard deviation above or below the mean.

Figure 5

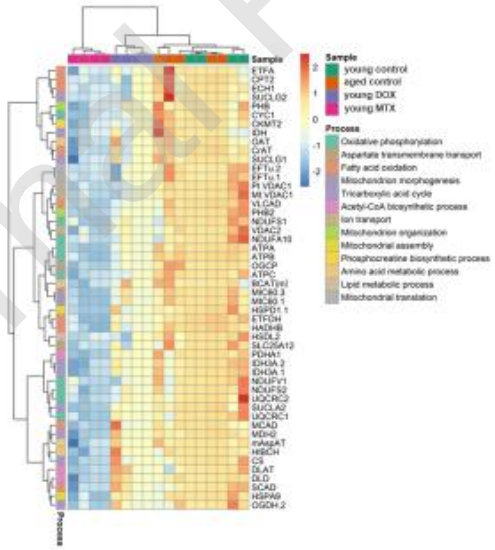

Figure 6. Boxplots for the top 16 proteins from mitochondrial enriched fractions of young control (CTRL, green), aged control (OLD, orange), young DOX (DOX, purple) and young MTX (MTX, pink) animals (n = 4 for young control, young DOX and young MTX; n = 5 for aged control). Statistical analyses were done by ordinary one-way ANOVA

followed by Tukey's multiple comparisons (* p<0.05, ** p<0.01, *** p<0.001, **** p<0.0001).

Figure 6

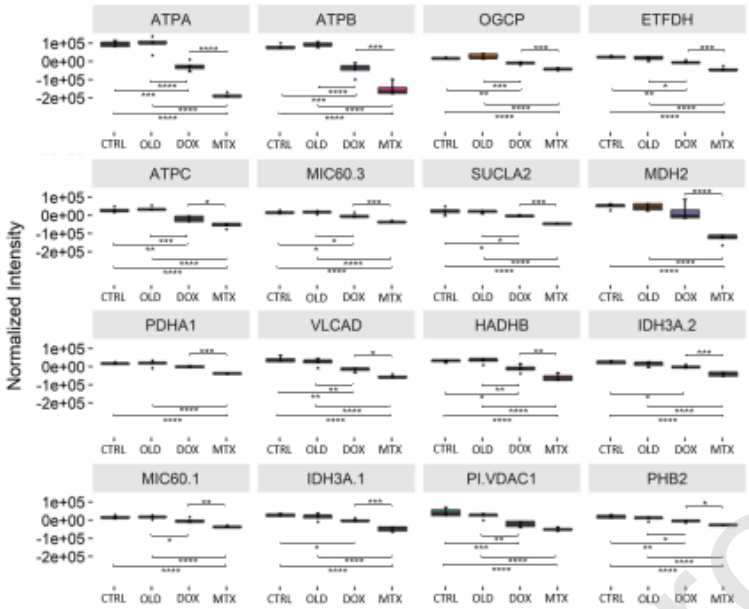

Figure 7. General overview of cardiac changes caused by doxorubicin (DOX) and/or mitoxantrone (MTX) and their interconnection in several pathways. Proteins indicated in orange were downregulated by both DOX and MTX, while the ones in blue were exclusively downregulated by MTX. Proteins in grey were not significantly modulated or were not in the top50 proteins evaluated herein. Figure made with *Servier Medical Art*. ACS: acyl-CoA synthetase; ATPA: ATP synthase subunit alpha; ATPB: ATP synthase subunit beta; ATPC: ATP synthase subunit gamma; BCAT(m): branched-chain-amino-acid aminotransferase; C-I: nicotinamide adenine dinucleotide-ubiquinone oxidoreductase; C-II: succinate dehydrogenase; C-III: ubiquinol-cytochrome c reductase; C-IV: cytochrome c oxidase; C-V: ATP synthase; CACT: carnitine/acylcarnitine translocase; CKMT2: creatine kinase S-type; CoQ: ubiquinone; CPT1: carnitine O-palmitoyltransferase 1; CPT2: carnitine O-palmitoyltransferase 2; Cr: creatine; CS: citrate synthase; CYC1: cytochrome c1, heme protein; Cyt c: cytochrome c; DLAT: dihydrolipoyllysine-residue acetyltransferase component of pyruvate dehydrogenase complex; DLD: dihydrolipoyl dehydrogenase; DLST: dihydrolipoyllysine-residue succinyltransferase component of 2-oxoglutarate dehydrogenase complex; ECH: 2-enoyl-CoA hydratases; EFTu: elongation factor Tu; ETFA: electron transfer flavoprotein subunit alpha; ETFB: electron transfer flavoprotein subunit beta; ETFDH: electron transfer flavoprotein-ubiquinone oxidoreductase; FAD: flavin adenine dinucleotide; $FADH_2$: reduced form of FAD; Glc: glucose; HADH: 3-hydroxyacyl-CoA dehydrogenases; HADHA: trifunctional enzyme subunit alpha; HADHB: trifunctional enzyme subunit beta; HIBCH: 3-hydroxyisobutyryl-CoA hydrolase; HSPA9: stress-70

protein; HSPD1: 60 kDa heat shock protein; IDH: isocitrate dehydrogenase; IDH3A: isocitrate dehydrogenase [NAD] subunit alpha; KAT: 3-ketoacyl-CoA thiolases; LACS: long-chain acyl-CoA synthetase; LC-carnitine: long-chain fatty acylcarnitine ester; LC-CoA: long-chain fatty acyl-CoA ester; LCFA: long-chain fatty acids; mAspAT: aspartate aminotransferase; MCAD: medium-chain specific acyl-CoA dehydrogenase; MC-CoA: medium-chain fatty acyl-CoA ester; MCFA: medium-chain fatty acids; MDH2: malate dehydrogenase; MIC60: MICOS complex subunit Mic60; mtDNA: mitochondrial DNA; NDUFA10: NADH dehydrogenase [ubiquinone] 1 alpha subcomplex subunit 10; NDUFS1: NADH-ubiquinone oxidoreductase 75 kDa subunit; NDUFS2: NADH dehydrogenase [ubiquinone] iron-sulfur protein 2; NDUFV1: NADH dehydrogenase [ubiquinone] flavoprotein 1; OGCP: 2-oxoglutarate/malate carrier protein; OGDH: 2-oxoglutarate dehydrogenase; PCr: phosphocreatine; PDHA1: pyruvate dehydrogenase E1 component subunit alpha; PHB: prohibitin; PHB2: prohibitin-2; Pi: inorganic phosphate; Pyr: pyruvate; SCAD: short-chain specific acyl-CoA dehydrogenase; SC-CoA: short-chain fatty acyl-CoA ester; SCFA: short-chain fatty acids; SDH: succinate dehydrogenase (C-II); SLC25A12: calcium-binding mitochondrial carrier protein Aralar1; SUCLA2: succinate--CoA ligase [ADP-forming] subunit beta; SUCLG1: succinate--CoA ligase [ADP/GDP-forming] subunit alpha; SUCLG2: succinate--CoA ligase [ADP/GDP-forming] subunit beta; UQCRC1: cytochrome b-c1 complex subunit 1; UQCRC2: cytochrome b-c1 complex subunit 2; VDAC1: voltage-dependent anion-selective channel protein 1; VDAC2: voltage-dependent anion-selective channel protein 2; VLCAD: very long

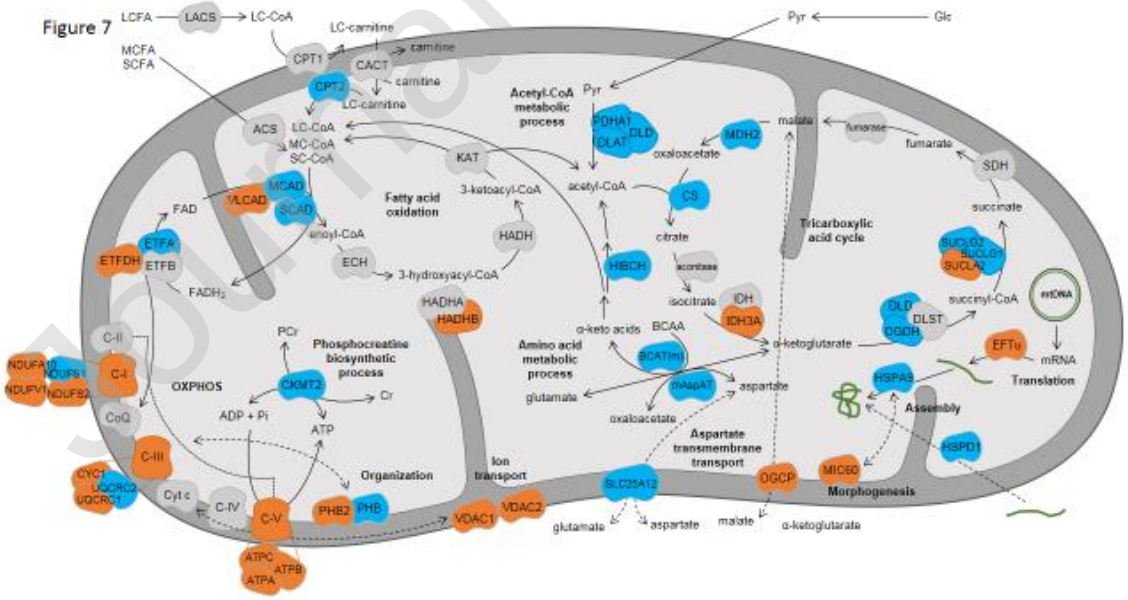

Table 1

Table 1. Whole-body weight (g), heart weight (g), brain weight (g), heart weight-to-brain weight ratio, heart weight-to-whole body weight (mg/g) at sacrifice, and heart mitochondrial isolation yield (mg protein/g tissue and mtDNA-to-tDNA) of young control, aged control, young DOX and young MTX animals.

		Experimental group			
		young control	**aged control**	**young DOX**	**young MTX**
Whole body weight (g)		45.93 ± 2.62	52.95 ± 6.67**	43.73 ± 2.76^{+++}	41.13 ± 1.68*, $^{++++}$
Heart weight (g)		0.33 ± 0.03	0.35 ± 0.04	0.27 ± 0.04*, $^{++}$	0.25 ± 0.06**, $^{+++}$
Brain weight (g)		0.45 ± 0.03	0.51 ± 0.02***	0.48 ± 0.02^{+}	0.48 ± 0.02
Heart weight-to-brain weight		0.75 ± 0.07	0.74 ± 0.06	0.57 ± 0.08***, $^{++}$	0.55 ± 0.11***, $^{++}$
Heart weight-to-whole body weight (mg/g)		7.22 ± 1.00	6.71 ± 0.59	5.98 ± 1.13	6.24 ± 1.39
Heart mitochondrial isolation yield	(mg protein/g tissue)	3.26 ± 0.70	4.03 ± 0.63	3.23 ± 0.90	3.72 ± 1.15
	(mtDNA-to-tDNA)	0.11 ± 0.01	0.07 ± 0.03	0.14 ± 0.07	0.10 ± 0.04

Values are expressed as mean ± SD (n = 7-9 for young control; n = 5-6 for aged control; n = 8-9 for young DOX and young MTX). The statistical analyses were done by ordinary one-way ANOVA followed by Tukey's multiple comparisons (* $p<0.05$ vs. young control, ** $p<0.01$ vs. young control, *** $p<0.001$ vs. young control, $^{+}$ $p<0.05$ vs. aged control, $^{++}$ $p<0.01$ vs. aged control, $^{+++}$ $p<0.001$ vs. aged control, $^{++++}$ $p<0.0001$ vs. aged control).

Supplementary material legends

Supplementary Table 1. Specification of the dilutions and catalog number for each primary antibody used as well as the sampled tested. Whole cardiac homogenates and mitochondrial enriched fractions were the samples considered and it is presented if they were (Yes) or were not (No) tested for each antibody.

Supplementary Table 2. List of the 583 proteins identified by GeLC-MS/MS on mitochondrial enriched fractions. For each protein, several parameters reported by Proteome Discoverer are presented. The biological processes were attributed according to Gene Ontology database on Uniprot (http://www.uniprot.org).
calc. pI: calculated isoelectric point; MW: molecular weight.

Supplementary Table 3. List of the proteins used for statistical analysis regarding GeLC-MS/MS of young control (CTRL, green), aged control (OLD, orange), young DOX (DOX, purple) and young MTX (MTX, pink) animals. Abundance values after the EigenMS normalization and pareto scaling are presented.

Supplementary Figure 1. Representative images of the (**A**) Western blots obtained for cytochrome c (Cyt c) and sarcoplasmic/endoplasmic reticulum calcium ATPase 2 (SERCA2) on whole cardiac homogenates (HT) and mitochondrial enriched fractions (MIT) with the corresponding molecular weight, to check the purity of mitochondrial enriched fractions (n = 2); (**B**) gels stained with Colloidal Coomassie Blue G250 to demonstrate the electrophoretic separation of proteins from mitochondrial enriched fractions of young control (CTRL), aged control (OLD), young DOX (DOX) and young MTX (MTX) animals. The grid indicates the borders of the protein migration zones.

Supplementary Figure 2. Citrate synthase (CS) and ATP synthase activities measured spectrophotometrically, and electron transfer flavoprotein-ubiquinone oxidoreductase (ETFDH), MICOS complex subunit Mic60 (MIC60), OXPHOS complexes subunits (complex I: CI-NDUFB8, complex II: CII-SDHB, complex III: CIII-UQCRC2, complex IV: CIV-COX1 and complex V: CV-ATPA) and ATP synthase subunit β (ATPB) expression evaluated by Western blotting on mitochondrial enriched fractions of young control, aged control, young DOX and young MTX animals. ETFDH, MIC60, Complex I, Complex II, Complex III, Complex IV, Complex V and ATPB content is presented after normalization to total protein with Ponceau S staining, and in percentage of young control group. Representative images of the Western blots and the Ponceau S staining obtained are presented for each protein. Values are expressed as mean ± SD (n = 8-9 for young control, young DOX and young MTX of CS and ATP synthase activities; n = 4-5 for aged control of CS and ATP synthase activities; n = 4-6 for ETFDH, complexes I to V, and ATPB; n = 3-4 for MIC60). The statistical analyzes were done by ordinary one-way ANOVA followed by Tukey's multiple comparisons.